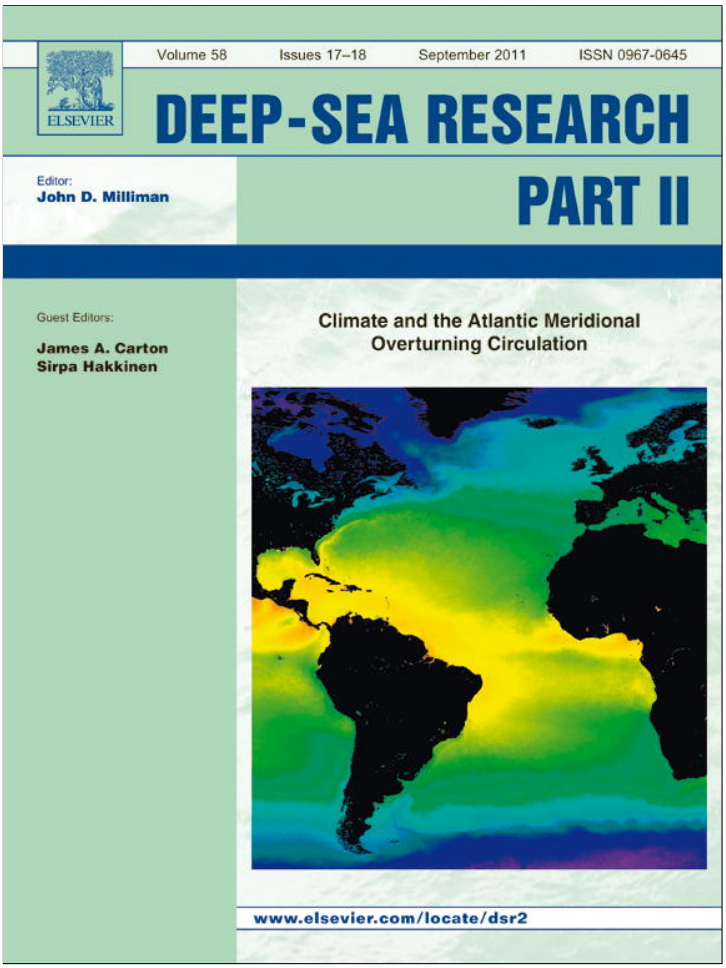

Deep-Sea Research II 58 (2011) 1858–1879

Contents lists available at ScienceDirect

Deep-Sea Research II

journal homepage: www.elsevier.com/locate/dsr2

Timescales and regions of the sensitivity of Atlantic meridional volume and heat transport: Toward observing system design

Patrick Heimbach [a,*], Carl Wunsch [a], Rui M. Ponte [b], Gael Forget [a], Chris Hill [a], Jean Utke [c]

[a] MIT, EAPS, Cambridge, MA, USA
[b] AER, Lexington, MA, USA
[c] ANL, Chicago, IL, USA

ARTICLE INFO

Article history:
Received 12 October 2010
Accepted 12 October 2010
Available online 19 February 2011

Keywords:
Meridional overturning circulation
Poleward heat transport
Decadal variability
Adjoint sensitivities
Dual state space
Observing system design
Oceanic teleconnections

ABSTRACT

A dual (adjoint) model is used to explore elements of the oceanic state influencing the meridional volume and heat transports (MVT and MHT) in the sub-tropical North Atlantic so as to understand their variability and to provide the elements of useful observational program design. Focus is on the effect of temperature (and salinity) perturbations. On short timescales (months), as expected, the greatest sensitivities are to local disturbances, but as the timescales extend back to a decade and longer, the region of influence expands to occupy much of the Atlantic basin and significant areas of the global ocean, although the influence of any specific point or small area tends to be quite weak. The propagation of information in the dual solution is a clear manifestation of oceanic teleconnections. It takes place through identifiable "dual" Kelvin, Rossby, and continental shelf-waves with an interpretable physics, in particular in terms of dual expressions of barotropic and baroclinic adjustment processes. Among the notable features are the relatively fast timescales of influence (albeit weak in amplitude) between 26°N and the tropical Pacific and Indian Ocean, the absence of dominance of the sub-polar North Atlantic, significant connections to the Agulhas leakage region in the southeast Atlantic on timescales of 5–10 years, and the marked sensitivity propagation of Doppler-shifted Rossby waves in the Southern Ocean on timescales of a decade and beyond. Regional, as well as time-dependent, differences between MVT and MHT sensitivities highlight the lack of a simple correspondence between their variability. Some implications for observing systems for the purpose of climate science are discussed.

1. Introduction

The need for understanding the physics of change in the ocean and their consequences for the global climate system are producing increasing calls for useful and sustained observing systems capable of quantitative description of the circulation. Useful systems are expensive to create, not easy to deploy and maintain, and *decisions made today about particular system design will largely determine what will be known of the ocean circulation for decades to come*—a major responsibility for those attempting to construct ocean observing systems. Thus, because of the considerable expense, and the long-term consequences, and in contrast with most of the history of physical oceanography, one seeks a better, prior, understanding of the capabilities of any particular system design—before commitments are made to actually deploy it.

The most difficult aspects of observing system design concern the questions of what should be measured, and how well such measurements must be made. By "well" is meant all of the usual considerations of accuracy, precision, sampling rates and space–time coverage underlying any system. Measurement purposes can be widely different. Are systems intended for "monitoring", "early warning", or for understanding? Is one concerned with detecting change over months or decades? Answers to these questions must account for cost–benefit ratios and the ease or difficulty of sustaining the system.

Different emphases affect the choice of an observing system. If one were interested in the meridional heat transport (MHT) or volume transport (MVT) at a given latitude in the North Atlantic, then producing a "now-cast" will likely put the focus on measuring variables in the vicinity of the latitude in question (in particular temperature T and meridional velocity v). However, if knowledge of the time history becomes relevant (annual to decadal and beyond) or "early warning" is a focus, it is conceivable that the strongest

* Corresponding author at: MIT, EAPS, Room 54-1518, 77 Massachusetts Avenue, Cambridge, MA 02139, USA. Tel.: +1 617 253 5259; fax: +1 617 253 4464.
E-mail addresses: heimbach@mit.edu (P. Heimbach), cwunsch@mit.edu (C. Wunsch), rponte@aer.com (R.M. Ponte), gforget@mit.edu (G. Forget), cnh@mit.edu (C. Hill), utke@mcs.anl.gov (J. Utke).

0967-0645/$ - see front matter © 2011 Elsevier Ltd. All rights reserved.
doi:10.1016/j.dsr2.2010.10.065

influence on changes in MHT or MVT will come through remote perturbations of various origins, whose influence superimpose, and whose propagation timescales (advective, wave-like, or diffusive) are relevant to the problem at hand.

The ocean is a fluid with a long memory. Thus changes in any particular variable at any particular location will result from the summation, and interaction, of phenomena potentially having occurred long ago and in remote locations. On long enough timescales, almost any oceanographic quantity of interest has to be considered as part of the global circulation and dynamically connected to it. Wunsch and Heimbach (2009) considered regions which dominate global meridional overturning circulation (MOC) variability on decadal timescales. That the ocean can transmit signals and changes over long distances and over extremely long times are well known. Examples are the dynamical calculation of baroclinic adjustment times by Veronis and Stommel (1956) and the multi-decadal sea-level adjustment timescales discussed by Johnson and Marshall (2002), Cessi et al. (2004), Stammer (2008), among many others. In the context of climate variability the problem has also been framed in terms of global oceanic teleconnections, e.g., Greatbatch and Peterson (1996), Cessi and Otheguy (2003), Johnson and Marshall (2004) and Liu and Alexander (2007). The tracer calculations by Wunsch and Heimbach (2008) and transit time or age distributions by, e.g., Holzer and Hall (2000), Haine and Hall (2002), Khatiwala (2007), Haine et al. (2008) and Primeau and Deleersnijder (2009) show that adjustment times of the ocean extend to millennial timescales and are completely global in scope.

To understand quantitatively the behavior of any regional oceanographic changes (e.g., local heat content, property transports through sections), one needs to know their sensitivity to non-local transients at various times and regions. In this paper, we begin the process of elucidating the space–time structure of the controls on oceanic changes of climate relevance for the purpose of evaluating potential climate observing systems. The basis for these calculations is the knowledge of the sensitivity of physical elements of oceanic GCMs to disturbances in both internal and external parameters and based on the powerful method of an adjoint model.

These methods are described in numerous references (e.g., Marotzke et al., 1999; Wunsch, 2006; Griewank and Walther, 2008; Heimbach, 2008) and are summarized in the Appendix. For present purposes, an adjoint model can be understood as a "dual" GCM, representing the flow of information in the GCM over all space and timescales. Related previous efforts are those of Marotzke et al. (1999) who considered a time span of only one year, Köhl (2005) who examined Atlantic MOC sensitivities to surface forcing and initial conditions at interannual timescales, and Bugnion et al. (2006a,b) whose emphasis was multi-centennial equilibrium estimates. The present focus is on seasonal to decadal timescales of climatologically important elements of the ocean circulation, and their spatial variations, that would influence decisions about the measurement systems necessary to understand their behavior. Although we do not specifically discuss the prediction problem, an implicit assumption is that prediction, if possible, necessitates both adequate understanding and observation of the most sensitive elements.

Consider by way of example the total meridional heat and volume transports across 26°N in the North Atlantic. These diagnostics can be computed as zonal ($\int \mathrm{d}\theta$) and vertical ($\int \mathrm{d}z$) integrals of instantaneous temperature T and meridional velocity v,

$$J_{MHT} = \frac{c_p \rho}{t_f - t_i} \int_{t_i}^{t_f} \int_{\text{depth}} \int_{\text{lon}} v(t) \cdot T(t)\, \mathrm{d}\theta\, \mathrm{d}z\, \mathrm{d}t, \quad \text{petawatts—PW}$$

$$J_{MVT} = \frac{1}{t_f - t_i} \int_{t_i}^{t_f} \int_{0\ \mathrm{m}}^{1200\ \mathrm{m}} \int_{\text{lon}} v(t)\, \mathrm{d}\theta\, \mathrm{d}z\, \mathrm{d}t, \quad \text{Sverdrups (Sv)—}10^6\ \mathrm{m}^3/\mathrm{s} \tag{1}$$

Choices of the times, t_i, t_f and the intervals of averaging, are at the disposal of the investigator and would normally reflect the purposes of the calculation. As a somewhat arbitrary reference for context here, December 2007 is chosen and the 1-month average values are $\bar{J}_{MHT} = 1.1$ PW and $\bar{J}_{MVT} = 14.4$ Sv, the overbar denoting the average values (instead of a 1-month average, a 1-year average could have been chosen; here we chose a 1-month average to exhibit more clearly the transient nature of the dual solution with respect to the objective function). The 1992–2007 mean values and standard deviations are $\langle J_{MHT} \rangle = 1.0 \pm 0.2$ PW and $\langle J_{MVT} \rangle = 13.8 \pm 2.9$ Sv for meridional heat and volume transports, respectively, with standard deviations calculated from monthly mean ensemble members.

The latitude of 26°N is approximately that of the maximum in North Atlantic MHT and is the focus of the RAPID/MOCHA mooring array which was deployed in 2004 (Cunningham et al., 2007; Kanzow et al., 2007) and which has been used to document fluctuations in the J on a variety of timescales accessible with a few years of data. Simple theory and models suggest that J_{MHT} and J_{MVT} will vary due to a variety of causes ranging from local fluctuations, e.g., in the wind field, to circulation variations that took place, e.g., in the Southern Ocean decades earlier, and which are now being manifest at 26°N. Should local fluctuations clearly dominate the changes in the J on all timescales, the oceanographic observation problem is clearly far simpler than if one must cope with a global set of influences. One cannot afford, however, to simply assume that dominance.

2. The method

The ocean model is that used in version 3 of the ECCO-GODAE state estimates (Wunsch and Heimbach, 2007; Wunsch et al., 2009). The model trajectory with respect to which sensitivities are calculated is one of the optimized ECCO-GODAE solutions for the period 1992 and 2007. Configuration details are found in the Appendix. The dual (adjoint) model was generated via the automatic differentiation tool TAF (Giering and Kaminski, 1998). To assess the robustness of the inferred sensitivities, results from a non-optimized solution are also presented (Section 3.5). The adjoint model for the non-optimized integration was generated both with TAF and with the more recently developed automatic differentiation tool OpenAD (Utke et al., 2008) for the purposes of testing the dual models against each other. The inferred sensitivities were found to be extremely similar. While a technical detail, the use of both TAF and OpenAD serves the purpose of demonstrating that MITgcm adjoint model generation can now be achieved with two independent AD tools.

Adjoint models are stable when integrated in the backward-in-time direction—corresponding to a determination of the propagation in space and time *from which* a disturbance at time t has emanated. Here the adjoint is integrated for 16 years backwards-in-time to January 1992. Formally, it furnishes the full set of time-varying Lagrange multipliers—which are equivalent to the sensitivities at each timestep, t. That is, if the forward model state vector is $\mathbf{x}(t)$, then to each element of the state $x_i(t)$, access is available to any dual variable, denoted as

$$\delta^* x_i(t) = \frac{\partial J}{\partial x_i(t)} \tag{2}$$

Snapshots every 15 days for various dual variables were saved for analysis. Here the focus is on elements of the oceanic state (temperature, salinity, pressure, and velocity). Equally important are sensitivities to the time-varying air–sea fluxes of momentum and buoyancy, but whose discussion we defer to a separate work

in the interest of keeping the wealth of material manageable, and point to recent work in this regard by Czeschel et al. (2010).

As can be seen in Eq. (1) the objective functions differ in that J_{MHT} computes correlated effects between the temperature and velocity fields over the full water column, whereas J_{MVT} is a plain measure of velocity effects over only the upper ocean, albeit the temperature weighting also gives emphasis to the upper ocean. Their sensitivities are thus expected to differ, in particular where zonally dependent temperature variations are significant.

A necessary consideration is how to assess the importance of regional sensitivities against each other, and the relative importance of sensitivities to different variables. First, recall that the sensitivities are related to actual changes in the objective function via the Taylor series expansion of J in the vicinity of a point x_{i0} of the form

$$J(x_i) = J(x_{i0}) + \left.\frac{\partial J}{\partial x_i}\right|_{x_0} \cdot (x_i - x_{i0}) + O(\|x_i - x_{i0}\|^2) \tag{3}$$

Eq. (3) suggests that a useful response estimate may be obtained from the gradients $(\partial J/\partial x_i)|_{x_0}$ by multiplying them with the actual anomalies, expected uncertainties in the observations, or the expected variability of x_i, i.e., $\sigma_i \sim (x_i - x_{i0})$.

The x_i are in practice components of different variables (such as temperature, salinity, surface forcing, model parameters) which we may distinguish via an index α, functions of time t and representative of three-dimensional vector fields; it is useful to acknowledge this specifically, by letting $i \to \alpha,i,j,k,t$. Then, using the three-dimensional a priori standard deviation fields $\sigma_\alpha(i,j,k)$ for each variable $x_\alpha(t)$, and rescaling the δJ in terms of their mean values $\bar{J}$, the "normalized response fields" per unit depth are

$$\delta\tilde{J} = \frac{1}{\Delta z(k)}\frac{\delta J(x_\alpha(i,j,k,t))}{\bar{J}} = \frac{1}{\Delta z(k)}\frac{1}{\bar{J}}\left.\frac{\partial J}{\partial x_\alpha}\right|_{(i,j,k,t)} \delta x_\alpha(i,j,k), \quad \text{where } \delta x_\alpha = \sigma_\alpha \tag{4}$$

Eq. (4) accounts for sensitivities (and perturbations) that, when discretized, are a function of thicknesses $\Delta z(k)$ at level k. To be able to compare the impact of relevant temperature perturbations independent of the thickness of the vertical level at which they are calculated, the gradient, Eq. (2) is now normalized by the level thickness $\Delta z(k)$. Resulting units are thus in normalized responses per unit depth, i.e., [1/m]. Standard deviation fields used here for temperature and salinity are the ones presented in Forget and Wunsch (2007). By way of example, Fig. 1 depicts $\sigma_T(i,j,k)$ for temperature ($\alpha = T$) at 222 and 847 m depths. In the remainder of this paper, "sensitivities" always refer to the *normalized* ones.

Other choices of δx are conceivable, two of which we briefly mention, and each of which has its merit. One is the use of optimal perturbation patterns, i.e., patterns that are obtained from an optimization problem in which the largest amplification of a specified norm (e.g., meridional volume transport) is sought. Thus, rather than expressing responses in terms of anomalies from "expected" uncertainties, anomalies are based on patterns that would lead to a maximum amplification. Such patterns, also called singular vectors, have recently been derived in an idealized GCM configuration by Zanna et al. (2010, 2011). The relationship between optimal patterns and expected uncertainty patterns remains to be explored in detail. Another approach would consist in calculating time-varying anomaly fields with respect to the mean over the model integration. MVT and MHT perturbations could then be reconstructed in terms of these anomaly fields. This approach was followed by Czeschel et al. (2010) who reconstruct AMOC changes from atmospheric perturbation anomalies in conjunction with adjoint forcing sensitivities.

3. Adjoint pathways and processes

The following provides a description of what could be termed a dual view of adjustment processes and timescales. Because of the correspondence of the adjoint model to the adjoint of a system of partial differential equations (e.g., Morse and Feshbach, 1953; Lanczos, 1961), the dual model can be described in terms of, among other phenomena, *adjoint* Kelvin (coastal and equatorial)

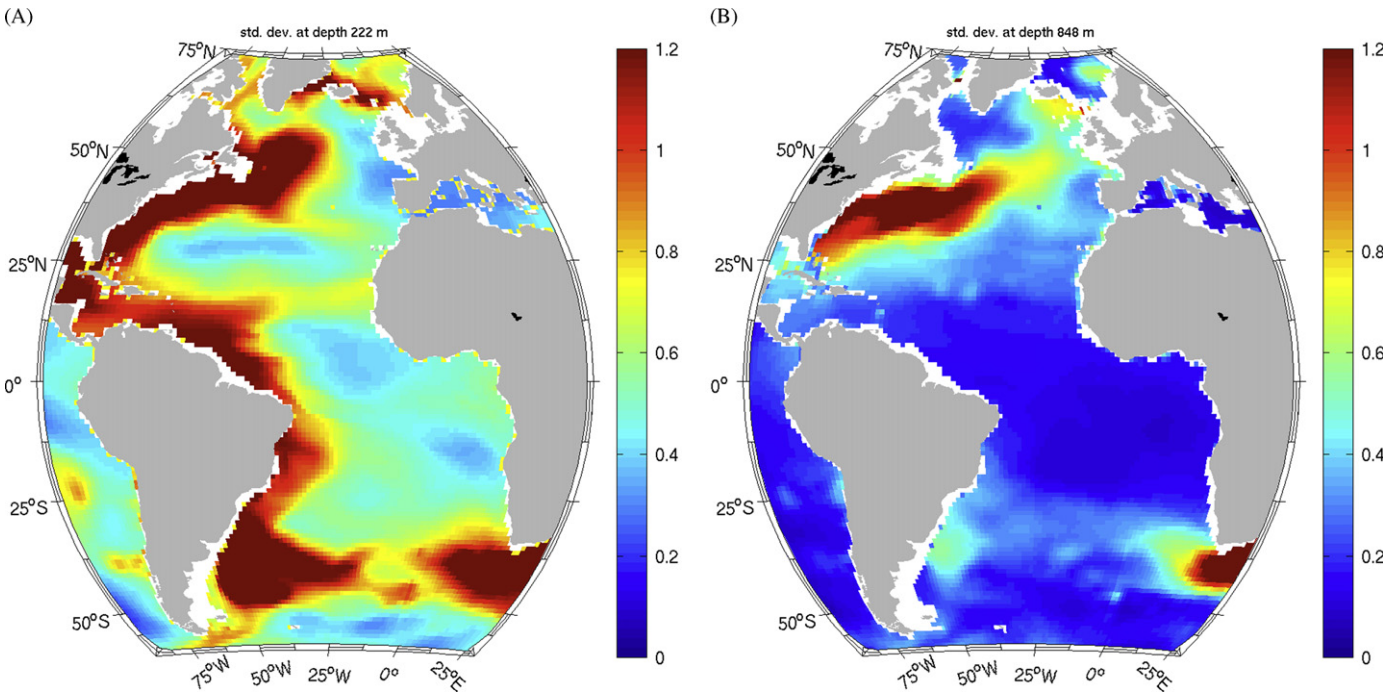

Fig. 1. Maps of uncertainty estimates of in situ observations for temperature in °C (but dominated by representation errors due to eddy variability) at different depth levels, based on Forget and Wunsch (2007), and used here to produce perturbation response estimates following Eq. (4): (A) 222 m depth and (B) 847 m depth.

and Rossby waves.[1] These determine the relevant pathways and timescales by which information is transmitted in the forward model (Galanti and Tziperman, 2003). A full discussion here of adjoint physics is not possible, but note, for example, that the forward model tends to produce westward-propagating Rossby waves from the eastern boundary, whereas in the dual model, it is the western boundary which generates eastward propagating analogs of Rossby wave physics (because information arrives at a point i,j,k at time t having traveled westward from further east, a backwards-in-time calculation of the region from which it arose involves propagation *eastward*).

Much of what follows is built on the descriptive result that the solution of adjoint wave problems is waves traveling in the opposite direction to their forward solution. To reinforce this perspective, the terminology of *dual* Kelvin, *dual* Rossby, or *dual* continental shelf-waves will be used. Schröter and Wunsch (1986) discuss the *dual* Gulf Stream, but the time-mean is not our present concern. Although adjoint models are linear ones, the reader will be aware that they are nonetheless full three-dimensional GCMs with all of the details and complexity of any other global scale fluid model, making the description of full solutions a considerable challenge.

3.1. Atlantic signatures with up to 4 years propagation time

To begin the discussion, we first focus on the accessible timescale of about 4 years preceding December 2007. Fig. 2 shows snapshots of MVT sensitivities to temperatures in the Atlantic from 0.1 years in the past back to 4 years earlier, at the depth of 222 m. After 4 years (bottom right panel), the MVT sensitivity pattern is the result of the superposition of different processes and various "centers of action" seem to affect MVT. A brief description of the results in Fig. 2 is now given, and Fig. 3 illustrates in a schematic way some of the main processes identified and described. Here, all times are given as years *before* December 2007.

- *0.1 year:* The strongest (normalized, i.e., scaled by σ, see Eq. (4)) sensitivities are centered around the 26°N section and are an expression of the fast barotropic processes that are the only ones able to affect MVT on very short timescales. These sensitivities persist throughout the entire water column with essentially the same pattern (not shown). Positive sensitivities extending southward from 26°N are prominent along the eastern boundary (labeled [E1]) and enter the equatorial wave guide off the Gulf of Guinea (Africa, off Cote d'Ivoire). Negative sensitivities are apparent along the western boundary, extending from 26°N to Flemish Cap (labeled [E2]). These patterns reflect the relatively fast connections along the boundaries provided by coastal Kelvin waves, which can exert control on MVT by changing pressure patterns near the eastern and western boundaries. Otherwise, sensitivities are also large near and along 26°N, reflecting Rossby wave processes that can affect the western boundary.
- *0.2 year:* The positive anomaly [E1] travels westward as an equatorial dual Kelvin wave through the equatorial wave guide, reaches the coast of South America (off Brazil) from where it sheds coastal dual Kelvin waves northward and southward into the corresponding hemisphere. A first notable consequence is that the positive response anomaly now visible off the South American coast (centered around French Guyana) is connected to 26°N, not via a western basin direct connection (short circuit), but rather via an eastern basin origin, having traveled from the eastern part of the basin (in adjoint sense) through the equatorial wave guide.

  A negative anomaly (labeled [E3]) is now visible off the African coast extending southward from 26°N, having propagated eastward as expected from dual Rossby waves. The negative anomaly along the western boundary [E2] reaches the Labrador Sea, remaining essentially coastally trapped.
- *0.5 year:* The negative anomaly [E3] which had traveled east and southward from 15°N along the African coast, enters the equatorial wave guide in the Gulf of Guinea. Positive anomaly [E1] that has spread as a coastal dual Kelvin wave along South American coast starts shedding dual Rossby waves into the interior. The mechanism for their reinforcement is likely similar to the one described by Galanti and Tziperman (2003) in the Pacific as delineating baroclinically unstable regions. Likewise, the negative anomaly along North America [E2] radiates dual Rossby wave into the interior. Weak signals start to appear off southern Greenland from [E2].
- *0.75 year (not shown):* Positive anomalies propagate as dual Rossby waves [E1] in a latitudinal band between 10 and 30°S are apparent, and having latitudinally dependent propagation speeds. Negative anomaly [E3] has crossed the equator, now triggering a dual coastal Kelvin wave along South America. The negative anomaly dual Rossby wave train [E2] in the eastern North Atlantic between roughly 10 and 30°N is also clearly visible. A dual coastal Kelvin wave (still linked to the original wave [E1]) reaches Cape Horn, surrounds it, and continues along the Chilean coast (not shown), illustrating the very fast link between the North Atlantic and the Southern Ocean through Kelvin wave dynamics. In a forward sense, a perturbation entering the South Atlantic through the Drake Passage is propagated equatorward as a coastal Kelvin wave, changes the side of the basin as an equatorial Kelvin wave, and connects northward to 26°N as a coastal Kelvin wave along West Africa.
- *1 and 2 years:* All the above processes continue to evolve (backwards) in time. Equatorward propagating coastal Kelvin waves are unable to cross the equator, but instead change sides of the basin in the equatorial wave guide before continuing poleward. The subsequent propagation of information to the western side through the interior is quite slow. This result confirms the idea of an equatorial buffer (e.g., Johnson and Marshall, 2002, 2004), although it should be noted that, despite the delay, the influence of the southeastern part of the Atlantic on these long timescales remains important. A signature of the β-effect in an adjoint sense is clearly visible, especially south of the equator where the positive lobe between 15 and 30°S shows a southwest-to-northeast tilt. This result is consistent with the basic properties of the corresponding *forward* Rossby waves whose phase speed increases towards the equator (e.g., Chelton and Schlax, 1996; Killworth et al., 1997).
- *3 years (not shown):* The positive dual Rossby wave trains from [E1] have reached the eastern part of the Atlantic basin, in the northern hemisphere bounded between 15 and 35°N off West Africa, in the southern hemisphere between 15 and 35°S off Namibia. Interestingly, there seems to be a northern barrier in the North Atlantic and a southern barrier in the South Atlantic. The origin of the latter is probably the Antarctic Circumpolar Current, whereas the origin of the former is not obvious. At least three possibilities exist: (1) Slow westward propagation of Rossby waves is Doppler-shifted through superposition with the mean flow associated with the sub-tropical gyre, the Gulf Stream and its North Atlantic current extension. (2) The dual

[1] The existence and use of "dual models" is commonplace in optimization theory of all kinds.

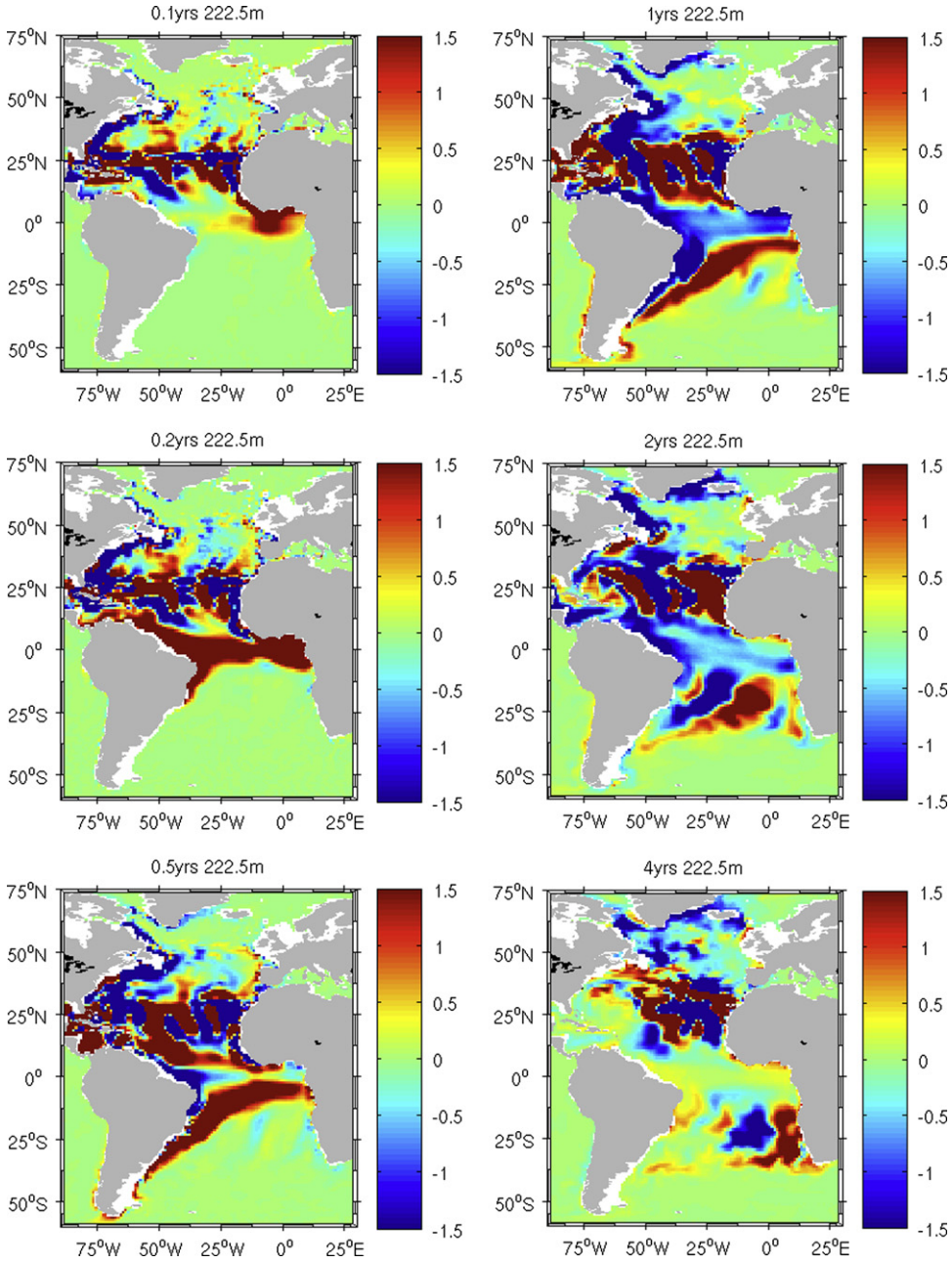

Fig. 2. Maps of normalized response fields of meridional volume transport, δJ_{MVT}, to temperature changes in the Atlantic at 222 m depth, calculated with the adjoint and using Eq. (4). From top-to-bottom-left to top-to-bottom-right they represent snapshots 0.1, 0.2, 0.5, 1, 2, and 4 years back in time. At each gridpoint the dual has been multiplied by the prior uncertainty estimate σ estimated by Forget and Wunsch (2007) and normalized by the cell thickness dz and by the value of J itself. Units are thus in [1/m], but rescaled by a factor of 10^7 for convenience.

Rossby waves need land in the east from which their forward counterparts are radiated. In the SH, the meridional extent is limited by the southern tip of Africa, in the northern hemisphere by the northern limit of Africa and the Strait of Gibraltar (Fukumori et al., 2006, based on adjoint calculations, have reported on basin-wide sea-level fluctuations in the Mediterranean due to fast boundary Kelvin waves). (3) The confinement may be associated with regions of baroclinic instabilities and where sensitivities are amplified in the sense discussed by Galanti and Tziperman (2003).

Another noteworthy feature is that dual Rossby waves seem to be absorbed at the eastern boundary—an analog of dissipative westward intensification in the forward dynamics. Some of it, however, likely arises from the generation of dual Kelvin waves at the coast.

- *4 years:* Apart from negative anomalies in the Labrador Sea and around Iceland, and other signals near the western boundary north of 26°N, which might suggest involvement of advective processes, most of the large sensitivities lie in the eastern part of the basins both for the North and South Atlantic. These are associated primarily with the slow propagation of dual Rossby wave trains along the 26°N section, and in the South Atlantic as relics from events [E1], [E3]. While sensitivities near 26°N might control the MVT by directly communicating interior perturbations to the western boundary, the connection to the eastern South Atlantic occurs through several processes.

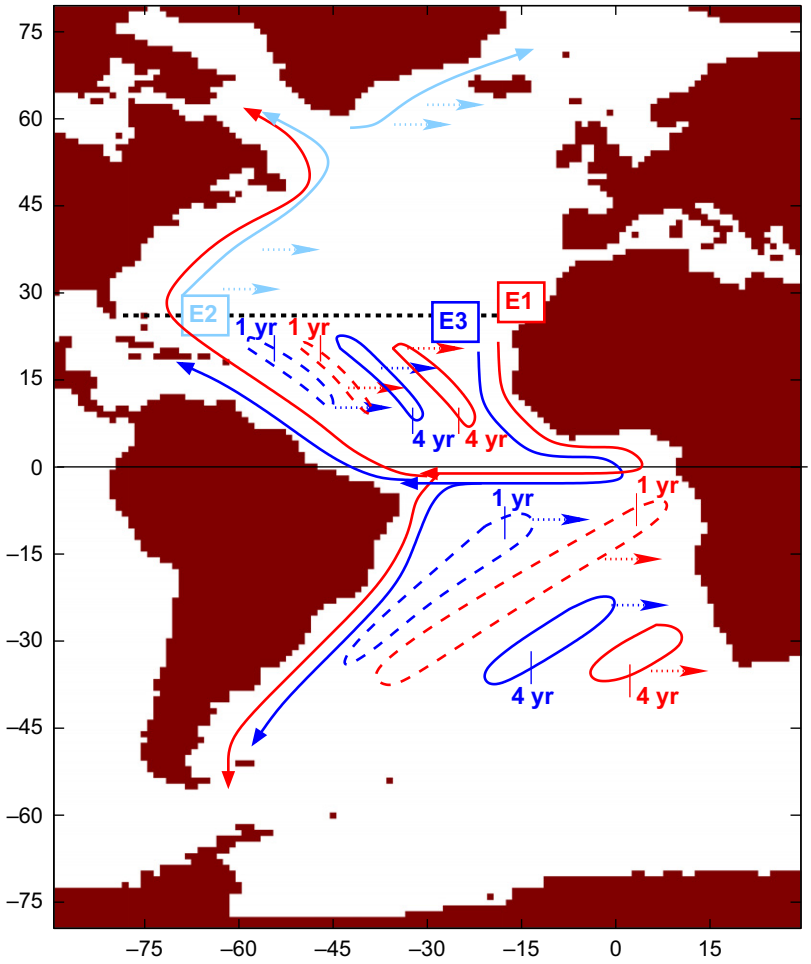

Fig. 3. A schematic of dual Kelvin waves (lines) and dual Rossby waves (contours and dotted arrows) propagating sensitivities from the 26°N line backward in time. Color coding refers to different events discussed in the text ([E1]: red, [E2]: light blue, [E3]: dark blue).

Perturbations near the southern tip of Africa (possibly triggered, e.g., via Agulhas leakage) can lead to forward Rossby waves, which are received off the coast of Brazil (after ~3 years), propagate towards the equator as coastal Kelvin waves, enter the equatorial wave guide and are propagated eastward as equatorial Kelvin waves, then northward along the West African coast, eventually connecting to 26°N on the eastern boundary.

Some of the mechanisms described for the near-surface (222 m) remain relevant near the base of the thermocline, e.g., at 847 m depth as depicted in Fig. 4; fast signal propagation through barotropic waves around 26°N, dual Kelvin waves, the equator serving both as barrier and wave guide, positive anomaly delivery off South America ([E1]), and fast negative anomaly propagation off North American coast ([E2]).

The South Atlantic dual Rossby wave signal is much weaker, presumably because 847 m is below the depth of the strongest baroclinic instabilities. In the North Atlantic a strong negative response signal emerges beyond 0.5 years. The interpretation is that of an efficient connection between 26°N and mid-latitude dual Rossby waves through coastal dual Kelvin waves. From a forward perspective, it points to a negative influence of Rossby waves carrying positive temperature anomalies at mid-latitudes. Once these anomalies reach the western boundary, they are efficiently transmitted to 26°N, where they effectively reduce the northward volume transport. At 30°S, eastward traveling dual Rossby waves which are prominent at 222 m depth, are still discernible at 847 m, but quite weak.

Maps similar to those depicted in Figs. 2 and 4 can also be produced for any prognostic variable, all of which possess dual variables (i.e., time-dependent Lagrange multipliers). In particular, *salinity* instead of *temperature* response maps were analyzed, but are omitted here for the sake of space. They show strong similarity in patterns, and the reversed sign indicates the opposite (compensating) effect of salinity and temperature on density and a basic sensitivity of MVT to density perturbations. These effects are not further discussed here, but they are clearly important in any discussion of controls on the circulation. A detailed discussion of density effects in an idealized Atlantic configuration is provided by Zanna et al. (2011) in the context of singular vector calculations. Response maps at depths will be further investigated in Section 3.7.

3.2. Amplitude-weighted timescales

A crude but useful way to infer transit times of response signals is to consider the amplitude-weighted mean time,

$$T_{tr}(i,j,k) = \frac{1}{N}\int_{t=0}^{16\ \mathrm{yr}} t|\delta J(i,j,k,t)|\ \mathrm{d}t \tag{5}$$

with normalizing factor $N(i,j,k) = \int_{t=0}^{16\ \mathrm{yr}} \delta J(i,j,k,t)\,\mathrm{d}t$. A spatio-temporally uniform δJ would result in a uniform $T_{tr} = 8$ yr. Maps of amplitude-weighted mean time at 222 and 1975 m depth

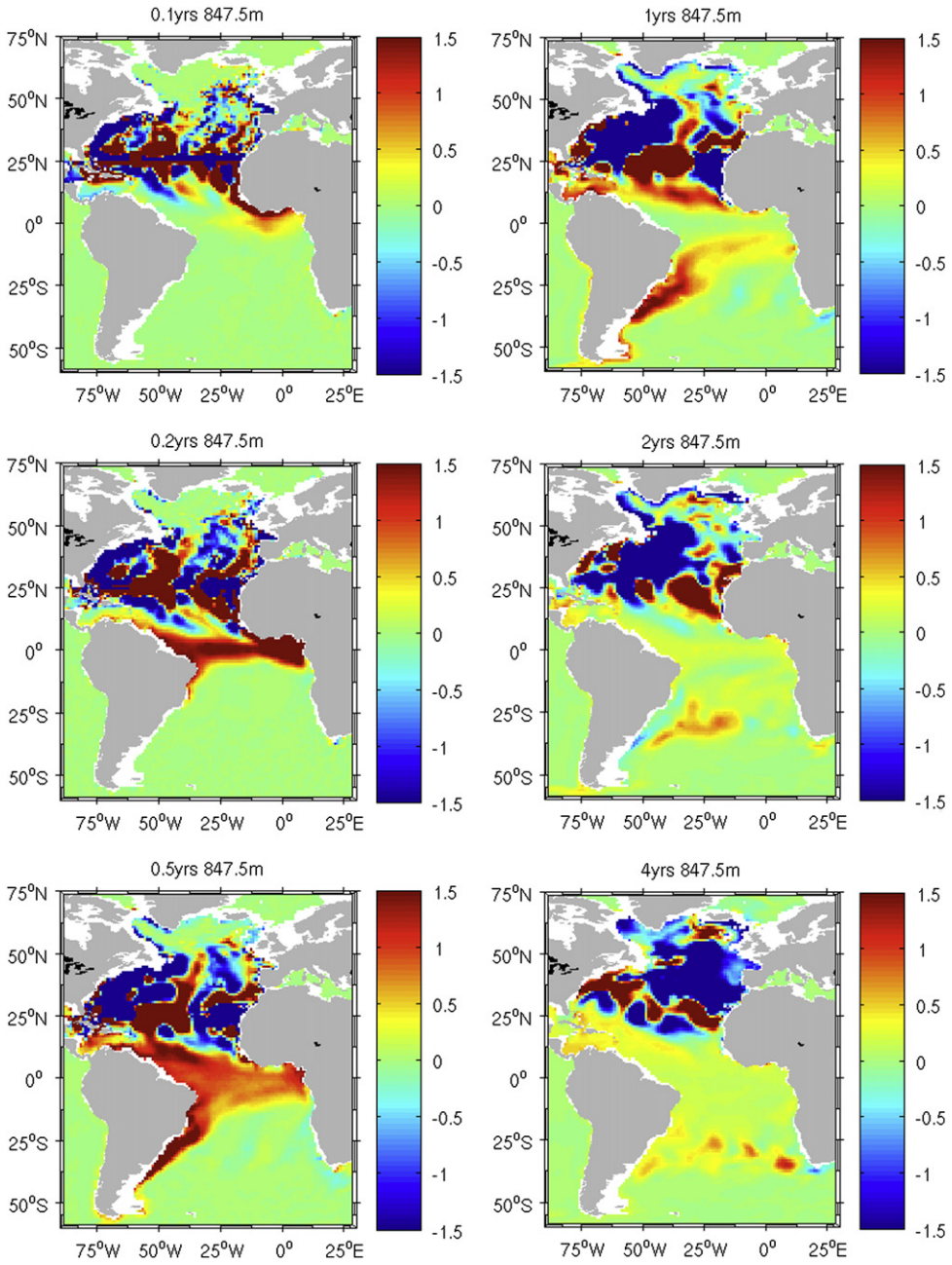

Fig. 4. Same as Fig. 2, but at 847 m depth.

(Fig. 5) clearly delineate fast timescales and pathways of sensitivities. Prominent features are

(1) localized sensitivities around 26°N (as expected);
(2) the Atlantic equatorial wave guide;
(3) the eastern seaboard of the Americas (North and South) as carrier of poleward-traveling dual Kelvin waves;
(4) sub-tropical Atlantic (5–35° latitude in both hemispheres) carrying dual Rossby waves;
(5) fast timescale motions leak through Drake Passage into the Pacific in the form of (a) dual Kelvin waves along the Chilean coast, entering the Pacific equatorial wave guide, changing sides of the basin as equatorial dual Kelvin waves, and shedding dual Rossby waves in the western Pacific, and (b) westward dual propagation in the Southern Ocean (to be discussed below), and likely the result of a Doppler-shifted westward-moving forward Rossby wave which is advected by a faster eastward-moving ACC;
(6) reduced timescales in the Indian Ocean are a consequence of a connection through fast dual Kelvin wave propagation along the South American coast, linked through the tropical Pacific wave guide into the tropical Indian Ocean;
(7) reduced timescale off the coast of Greenland.

Most noticeable in terms of the longest timescales are (i) the Nordic Seas (but whose interpretation is cautioned in view of the lack of an Arctic ocean in the model), and to some extent the central North Atlantic (surprising given the relative proximity to the 26°N section and suggesting an important long-term influence on MVT at 26°N); (ii) the eastern sub-tropical Pacific; (iii) the Southern Ocean south of the ACC. As a note of caution, the maps discussed here do not necessarily reflect *significant* regions of influence, because some

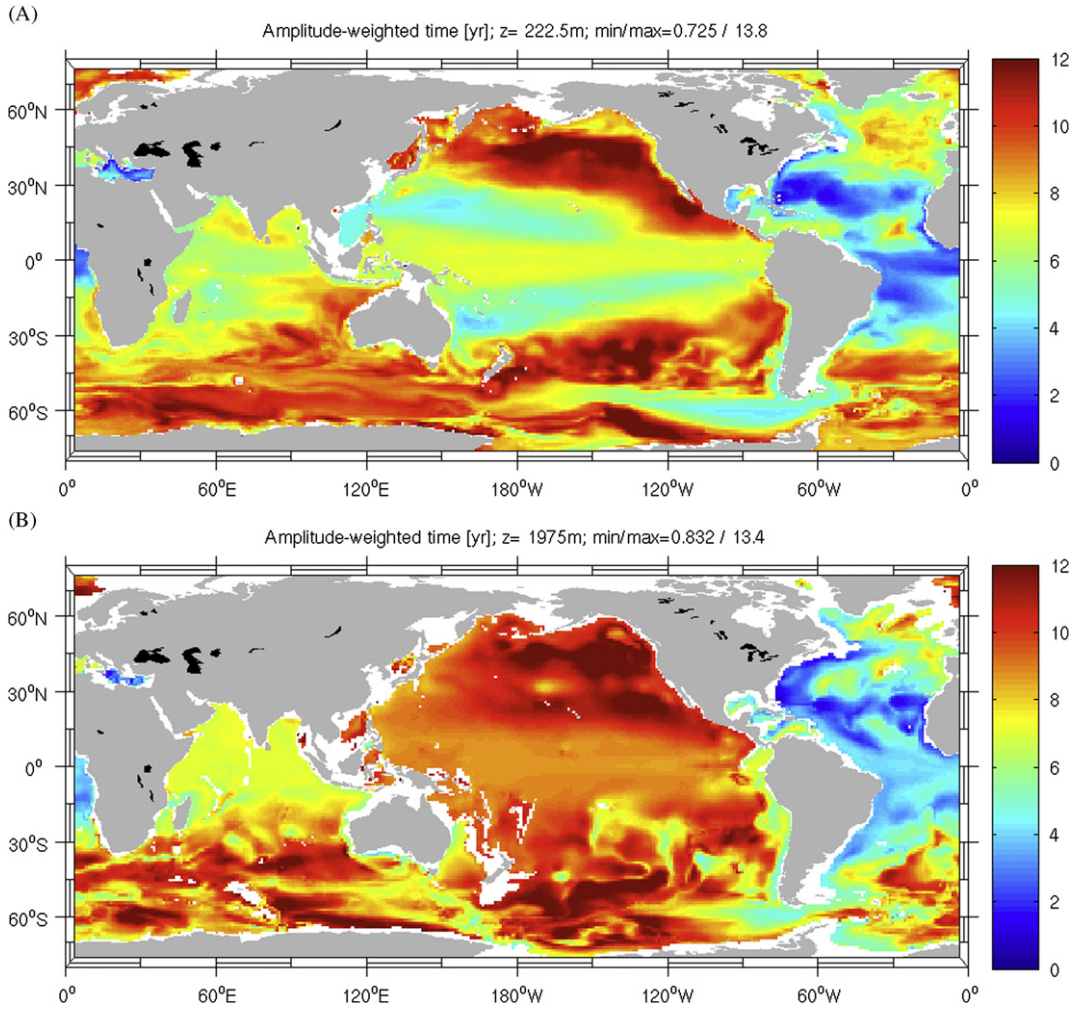

Fig. 5. Maps of mean times weighted by the amplitude of the normalized response fields, Eq. (5), for two different depth levels. Color scale refers to years (from 0 to 12). A small value in a certain region indicates fast dominant timescales of dynamical link between the region considered and 26°N in the Atlantic: (A) 222 m depth and (B) 1975 m depth.

of the very short timescales of influence may be associated with very low amplitudes of sensitivities (e.g., the tropical Pacific signal). Nevertheless, they do represent robust coherent patterns with underlying dynamical origins.

3.3. Zonal and meridional sections through time

Further evidence for zonal propagation of sensitivities comes from the analysis of longitude vs. time diagrams at a given latitude and depth. Figs. 6 and 7 depict such diagrams for MVT and MHT sensitivities, respectively. As an example, consider in Fig. 6 the panel representing MVT sensitivities at 27.5°N at 222 m depth (left column, third row). A wave-like dipole pattern hints at an eastward traveling dual Rossby wave which crosses the Atlantic in roughly 7–10 years. Similar patterns are visible at 1975 m depth, both at 27.5 and 41.5°N. The near-surface 41.5°N panel exhibits significant sensitivities in the western part of the basin out to 15 years back in time, but which apparently do not cross the entire basin in a similar fashion. A possible cause is the interaction of waves with a sheared flow in parts of the basin, and which may alter the dual propagation speed.

Further north, the comparatively weak sensitivities at 57.5°N are perhaps surprising, given the prominence in the literature attributed to this region in influencing the MVT. One apparent result is that at no time do high-latitudes dominate the sensitivities (notice though the limitation of absence of an Arctic ocean in the model).

In the southern hemisphere, the section at 28.5°S (bottom panel) reveals the dual Rossby wave crossing the South Atlantic, taking about 5 years to do so, and providing a dynamical link between the Agulhas leakage region and 26°N. The signal is prominent at 222 m depth, but essentially absent below the thermocline (1975 m depth), suggesting a weakened influence of the South Atlantic at depth both for MVT and MHT sensitivities (bottom panels of Fig. 9).

Finally, the panel at 1°S clearly shows the equatorial wave guide as the fastest connector between eastern and western Atlantic. Comparing Figs. 6 and 7 reveals similarities and differences between the MVT and MHT response patterns. These will be discussed in more detail in the context of latitude–time sections, but note, for example, large patterns of opposite signs for 1°S and 27.5°N at 222 m depth, or differences in patterns at 27.5°N at 1975 m depth.

Normalized responses are plotted in Fig. 8 as Atlantic time–latitude diagrams along fixed meridians (top panels: 45°W, bottom panel: 15°W). Also shown in Fig. 9 are panels representing the progression through time of the zonally integrated sensitivities at each latitude at 222 m (top panels) and 1975 m depth. Both figures show MVT sensitivities in the left column and MHT sensitivities in the right column. Note that while strong sensitivities might be present at fixed meridians and at certain latitudes (consider, e.g., the

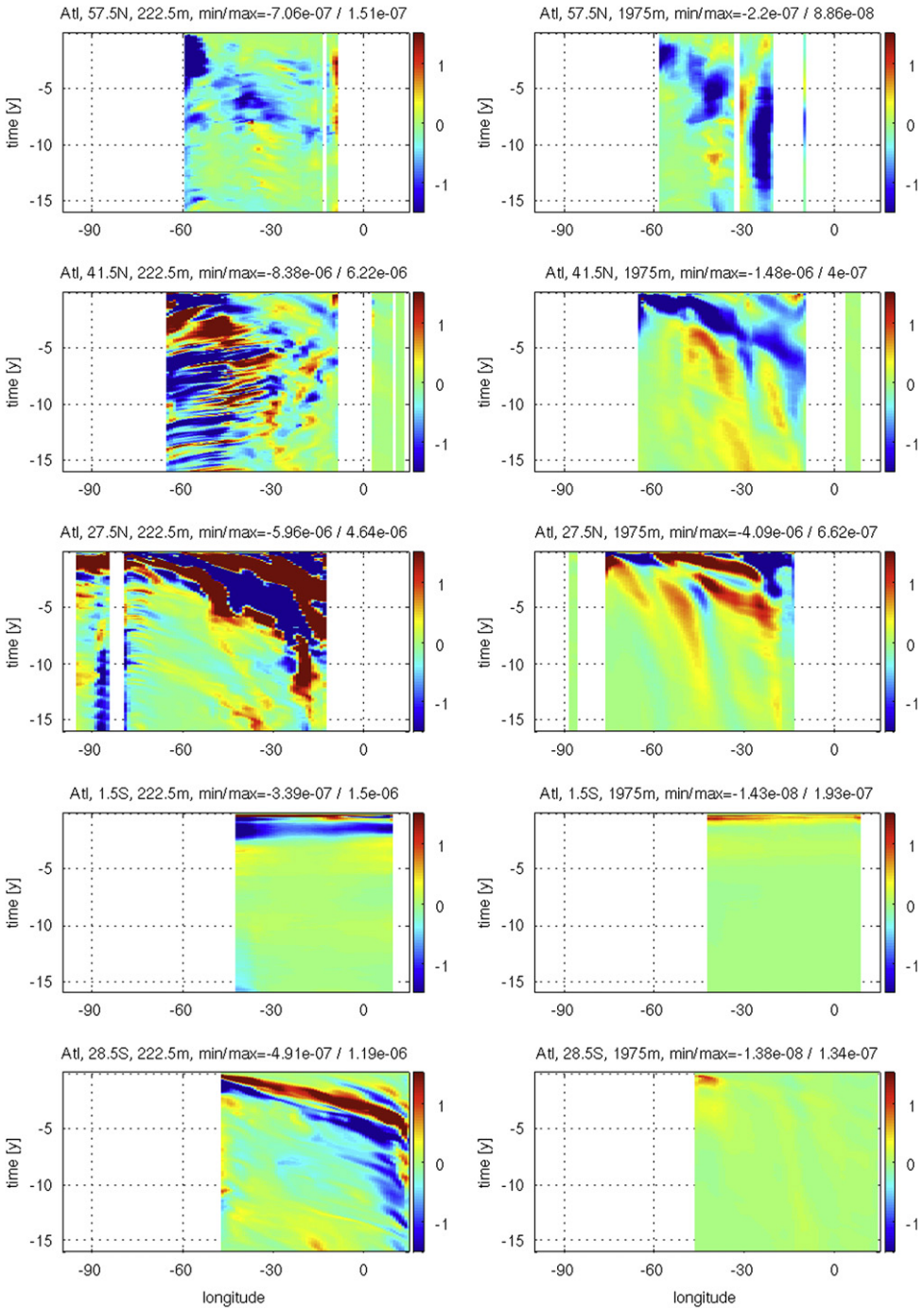

Fig. 6. Normalized MVT responses plotted as a function of longitude and time at various latitudes (from top-to-bottom: 57.5°N, 41.5°N, 27.5°N, 1.5°S, 28.5°S), and depths (left: 222 m, right: 1975 m). The sensitivities were calculated via Eq. (4). The negative time axis reflects integration backwards of the adjoint model from the evaluation time of the MVT diagnostic ($t=0$ yr).

prominent positive MVT sensitivity at 35°N, 15°W, between roughly 4 and 10 years in the bottom left panel of Fig. 8), the zonally integrated effect at this latitude is considerably weaker, if not reversed (top left panel of Fig. 9).

3.4. Meridional coherence

In the thermocline, an important (positive) contribution from southern latitudes up to about 10 years back in time is clearly visible. Also apparent is the negative influence from sub-polar regions (poleward of 45°N). The "boomerang" shape reflects the reduction of speed of dual Rossby waves with latitude, likely an effect of advection by the mean flow (Gulf Stream and North Atlantic current). This meridional change in character of sensitivities, in particular the increase in timescales of influence with latitude is consistent with findings by, e.g., Bingham et al. (2007). Their study finds a lack of meridional coherence of the AMOC, with a prominence of decadal variability north of roughly 40°N in contrast to higher frequency fluctuations to the south. Our findings support their caution in interpreting MOC variations recorded at any one latitude. The mechanisms revealed here in terms of the time-evolving dual fields may help shed light on the causes of meridional sensitivity structure.

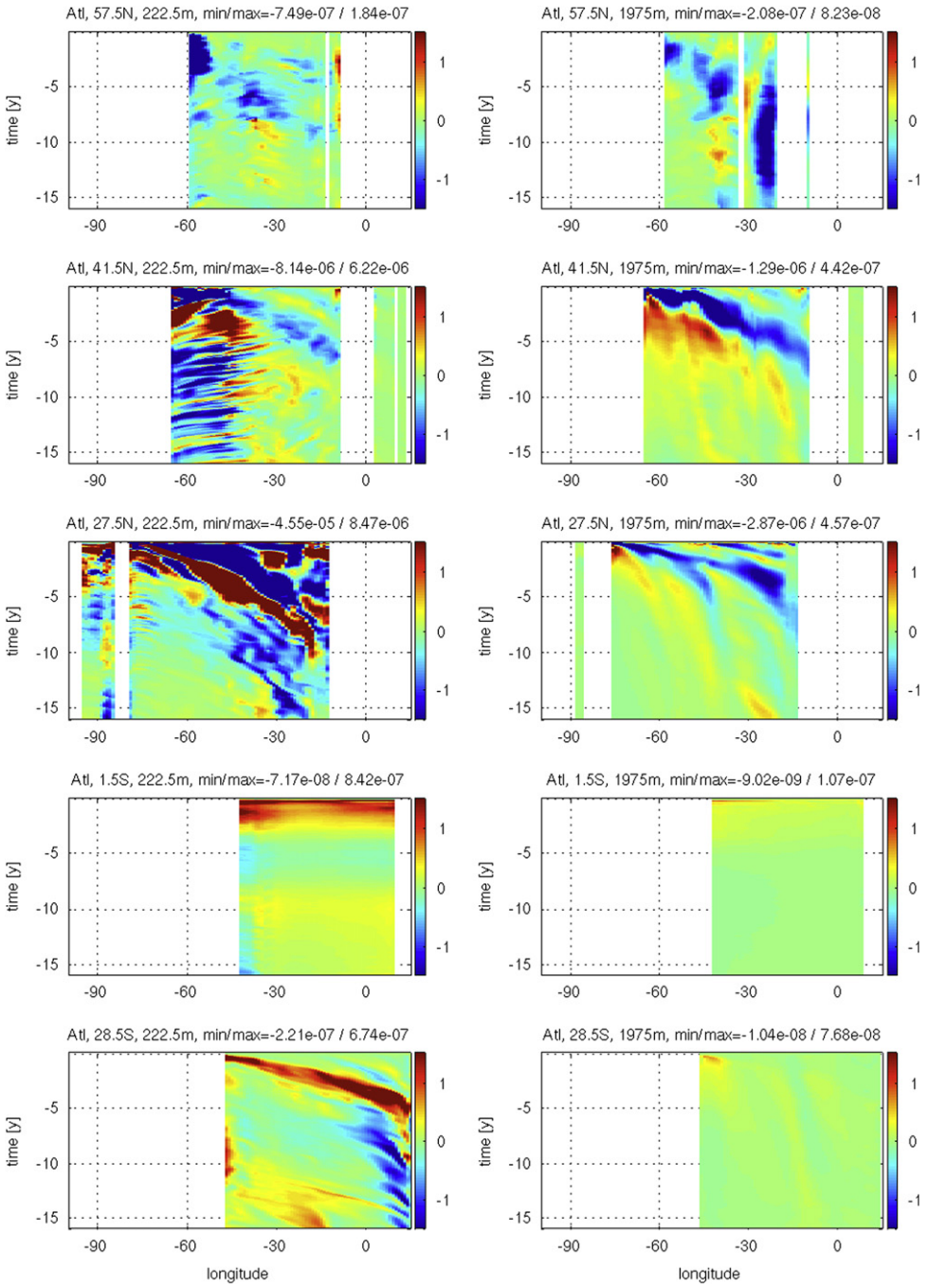

Fig. 7. Same as Fig. 6, but for normalized MHT responses.

A different way to assess the meridional coherence of the MVT is through a separate adjoint calculation of MVT sensitivities evaluated in the sub-polar gyre at 48°N, instead of 26°N. A sample result of such a calculation is depicted in Fig. 10, showing response maps to temperature perturbations at 222 m depth, which can be readily compared to corresponding response maps shown in Fig. 2 for the 26°N adjoint calculation. The corresponding long-term mean MVT at 48°N is $\langle J_{MVT} \rangle = 15.3 \pm 2.5$ Sv. The most striking differences are the much reduced response amplitudes in the sub-tropical gyre for the 48°N case, and an increased response north of Island. A time-lag of roughly half a year between 26 and 48°N calculation in tropical responses is also apparent. A robust feature in both calculations is the response pattern in the southeast Atlantic 4 years back in time.

The example serves to underline previous findings of a lack of meridional coherency of the MOC in the North Atlantic, a fact that needs to be taken into account when choosing climate-relevant target norms for sensitivity calculations, and when inferring of regions of dominant responses.

3.5. *Meridional volume vs. heat transport*

Fig. 9 allows for a comparison of time–latitude responses for MVT and MHT. The response fields calculated via Eq. (4) are normalized so as to provide a basis for comparison, both among responses to different variables, as well as between the MHT and MVT responses. Of particular interest is an assessment of the extent to which

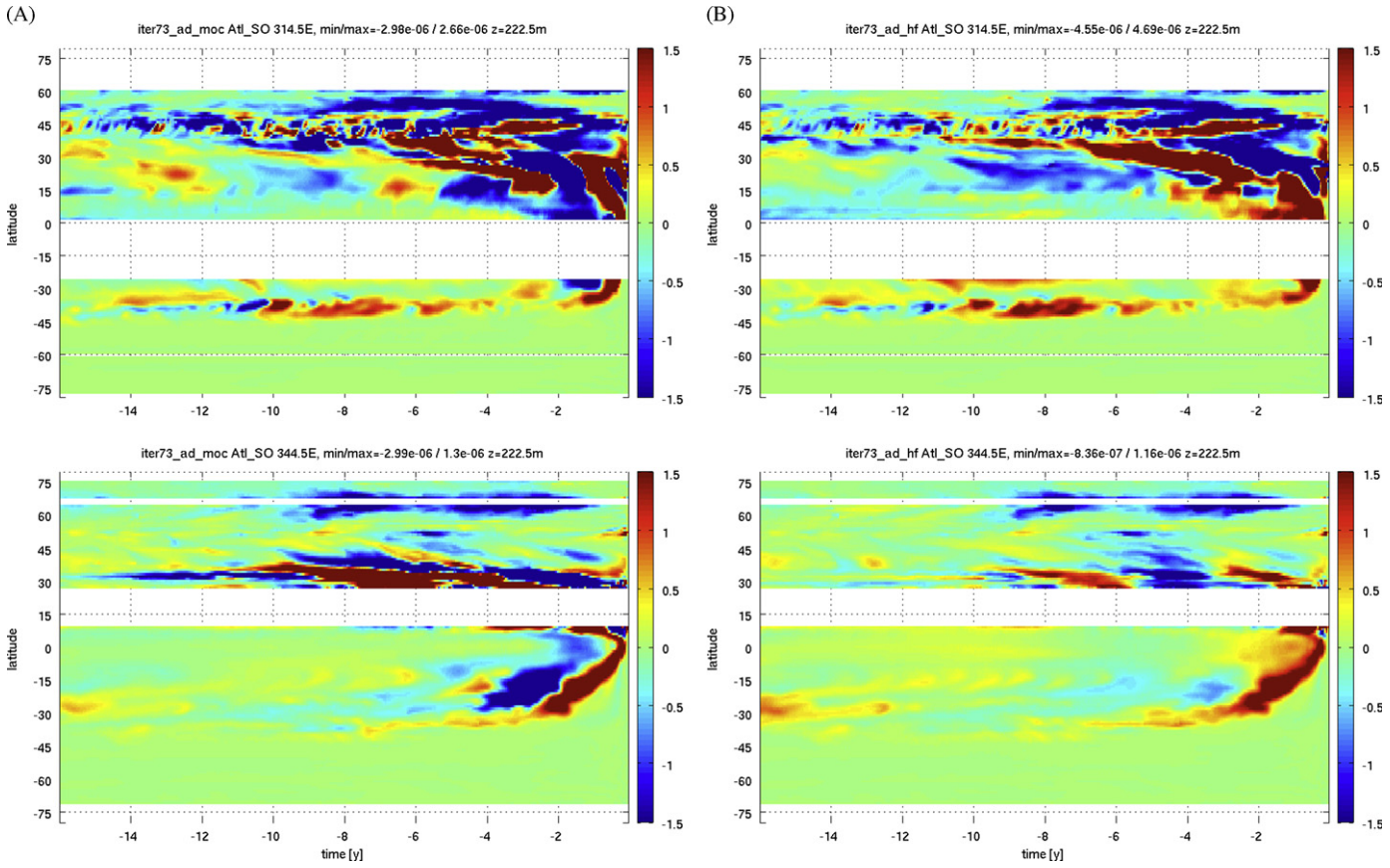

Fig. 8. Normalized responses for MVT (A) and MHT (B) at 222 m depth at fixed longitudes 45°W (top) and 15°W (bottom), as a function of time and latitude.

response patterns for MVT correspond to those for MHT. In other words, we wish to know whether responses in MVT to, e.g., temperature perturbations, result in correlated responses to MHT changes. For the sake of example, we focus on the zonal sum patterns (bottom panels) for MVT (A) vs. MHT (B).

Because δJ_{MHT} and δJ_{MVT} have been normalized (both with respect to their respective means $\bar{J}$ and with respect to the perturbation applied estimated through in situ variabilities σ) so as to be of similar magnitudes for the same perturbation applied, see Eq. (4), we can obtain a first crude impression by simply subtracting these normalized fields and scaling the residual obtained against the range of the field, thus

$$R(lat,t) = \frac{1}{\gamma}(\delta J_{MHT} - \delta J_{MVT}) \tag{6}$$

with a range value of $\gamma = 5 \times 10^{-6}$. The result is plotted in Fig. 11 for 222 m (top) and 1975 m depth (bottom). In the figure we have suppressed all signals for which the range of δJ_{MHT} itself is less than 20% of γ to focus on sizable signals only.

Small values of $R(lat,t)$ indicate latitudes (and times), where δJ_{MHT} and δJ_{MVT} act synchronously, i.e., increase in one variable corresponds to a (scaled) increase in the other. The most prominent such region is the North Atlantic, poleward of about 40°N out to 10 years, during which the responses have a sizable impact at 26°N.

In contrast, large (absolute) values in the figure correspond to latitudes (and times) for which the response of δJ_{MHT} is of opposite sign to that in δJ_{MVT}, or strong response in one quantity is not matched by a comparable response in the other, or the two lag each other. For example, temperature perturbations in the tropical Atlantic (15°N–15°S) are persistently of opposite sign out to roughly 3 years, with δJ_{MHT} being positive and δJ_{MVT} negative (Fig. 9). In the latitudinal band between roughly 15 and 40°N there is a very pronounced sign change in $R(lat,t)$. Interpretation in the context of monitoring, then suggests that observations of temperature anomalies at, e.g., 26°N, would have quite different consequences for transport estimates at the same location if taken 2 years ahead vs. those taken 4 years ahead.

3.6. Optimized vs. non-optimized solution

The question of the importance of the basic state (the model trajectory) with respect to which the *tangent* linearization is performed deserves attention. In other words, which response patterns are robust and independent of the model trajectory, and which aspects are highly dependent upon it? This issue is addressed by revisiting the MHT responses (Fig. 7) plotted as a function of time vs. longitude at various latitudes and depth levels, but for a non-optimized solution. The dual solution of the non-optimized trajectories was calculated somewhat differently from the optimized dual: the Large et al. (1994) KPP vertical mixing parameterization scheme has been omitted from the forward (and dual) model so as to permit an exact adjoint calculation (the adjoint of the full KPP scheme is unstable in parts); in contrast, the Gent–McWilliams/Redi parameterization (Gent and McWilliams, 1990; Redi, 1982) has been retained both in the forward and in the dual (note that in the optimized solution used here, both KPP and GM/Redi are turned off in the reverse integration, making the dual model an approximate linearization); and the integration period was extended to 20 years, i.e., the dual was integrated from December 2007 back to January 1988. (The constrained solution runs from 1992 forward—because that is when the database becomes of useful size with the advent of satellite altimetry.) Admittedly, the model configurations differ in a relatively large number of features, thus putting a severe test on the

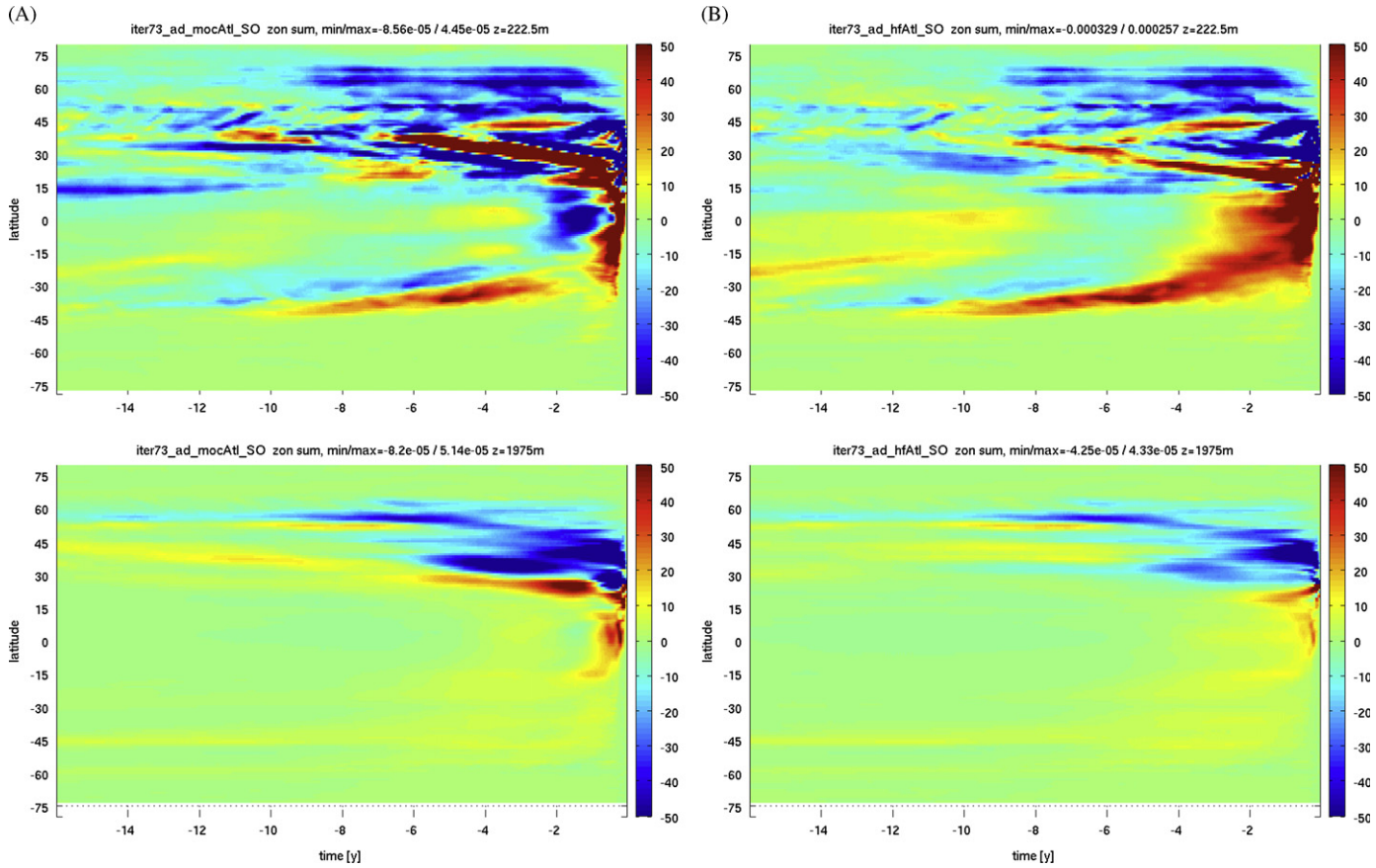

Fig. 9. Same as Fig. 8, but for the zonally integrated sensitivities (rather than those at particular longitudes) in the Atlantic: (A) MVT and (B) MHT.

dual solution's robustness. Nevertheless, the differences chosen here are typical across different model setups encountered, such that their comparison is warranted. In contrast to the optimized solution, the dual model for the non-optimized run has been generated both with the AD tool TAF (Giering and Kaminski, 1998) as well as with the new open-source AD tool OpenAD (Utke et al., 2008), and both models yield the same result.

Fig. 12 is a comparable plot to Fig. 7, but for the non-optimized model trajectory. Comparing the two figures, the normalized responses for the non-optimized trajectory show smoother signal propagation compared to the optimized trajectory. Nevertheless, most of the patterns can be readily identified in both solutions in terms of their broad structures, pointing to robust large-scale processes underlying the propagation mechanisms. In particular, all aspects discussed in Section 3.3 remain valid (albeit with slightly different amplitude) for the non-optimized solution. Additional aspects are perhaps somewhat easier to discern owing to the smoothness of the signal. For example, at depth (right column) one sees a pronounced increase and broadening of the tilt of negative sensitivities in going from 27.5 to 41.5 to 57.5°N, indicative of the β-effect. What appears to be noise in the left panels (e.g., at 57.5°N) is in fact an expression of the influence of the seasonal cycle in the near-surface (222 m depth) fields.

The noise in the near-surface panels (222 m, left column) can in part be explained by the influence of the boundary layer scheme that is present in the optimized calculation, but not in the non-optimized calculation (e.g., the effect of wind-induced deepening of the boundary layer). The second source of "noise", in particular at depth (right column) might stem from the influence of the observations to which the model was fit. The loss of smoothness may be interpreted as an attempt of the optimization to fit noisy observations, but to some extent it is also an expression of the eddy-rich context in which these observations were collected. One interpretation is that the smooth signal (or sensitivity) propagation apparent in the non-optimized solution is an "optimistic" limit (in the sense of how well dual signals may be discerned and tracked) of actual signal propagation in the real system in which smooth propagation will interact with the eddy field, and be obscured as a consequence.

3.7. *Abyssal processes and signatures beyond 10 years*

Further analyses have been performed for depth levels of 1975 and 2950 m. In general, normalized response signals (which are provided per unit depth) tend to diminish. By way of example, we revisit Fig. 6 (optimized solution) now focusing on the right column which depicts zonal sections vs. time along several latitudes in the Atlantic at 1975 m depth (corresponding panels for the non-optimized solution which are less noisy are in Fig. 12). It is apparent that the near-surface propagation in the South Atlantic is absent at depth. In the northern hemisphere, the "tilt" of sensitivity bands can be attributed to wave propagation, with an increase in tilt reflecting a decrease in propagation speed. This type of analysis may give some hints on where deep observations may matter for decadal-scale signal detection from long-term observations. For example, sensitivities of the 26°N transports to perturbations near 26°N subside beyond roughly 5 years, but remain significant further north out to 10 years and beyond. In the South Atlantic, no sizable sensitivities remain at depth beyond roughly 1 year.

Beyond 10 years backwards-in-time, sensitivities generally weaken but are more widespread. Near the surface, the dominant areas of influence remain confined to the Atlantic. However,

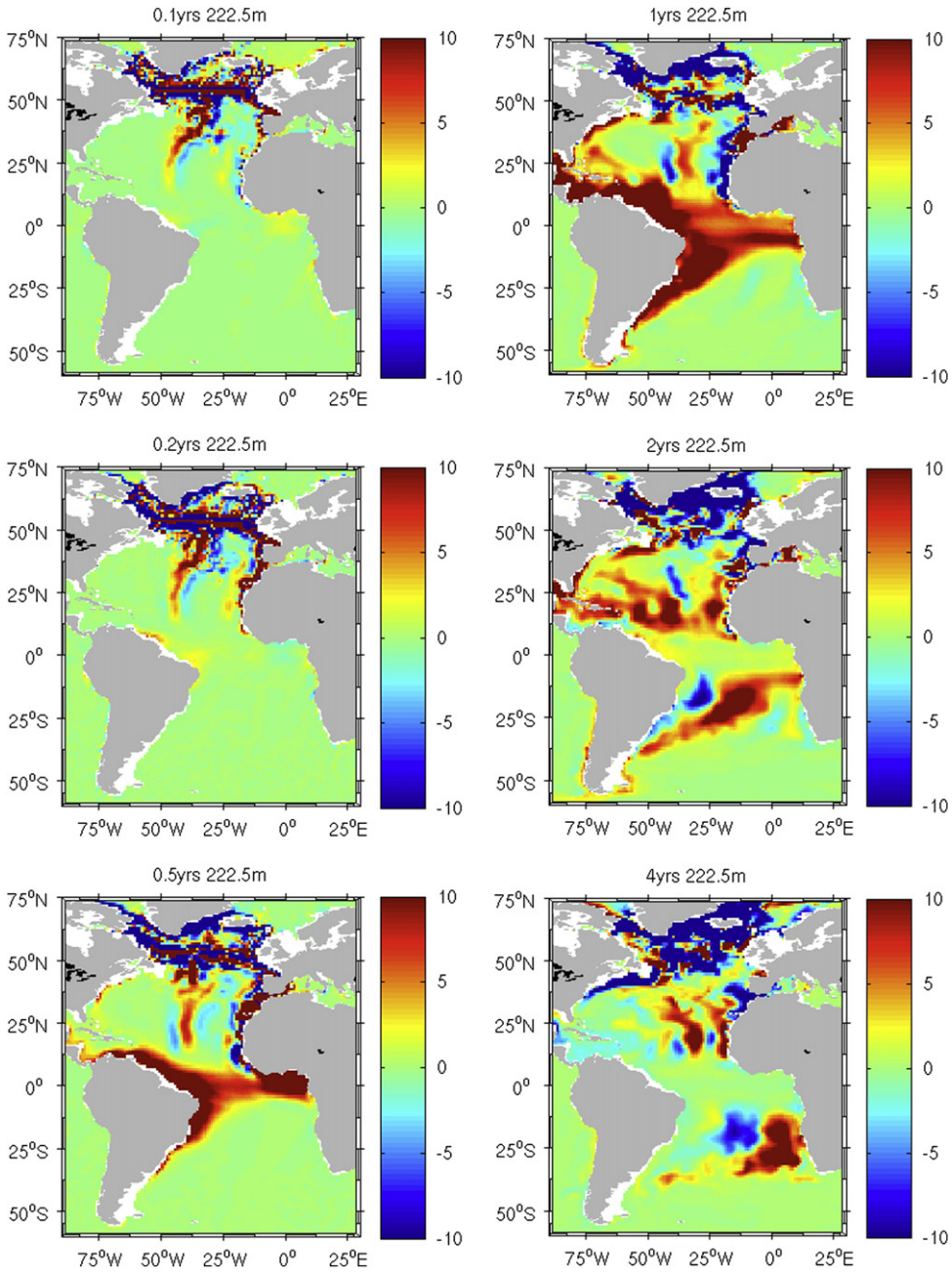

Fig. 10. Maps of normalized temperature response fields of meridional volume transport, δJ_{MVT}, similar to Fig. 2, but for MVT at 48°N, in the Atlantic at 222 m depth. Panels and units are as in Fig. 2.

below roughly 2000 m depth, a band of sensitivities throughout the Southern Ocean emerges after 10–15 years (e.g., Fig. 13 showing maps at 1975 and 2950 m depth, 15 years back in time), whose magnitudes are of comparable size to Atlantic sensitivities at the same depth and time. The MVT and MHT response maps look similar (not shown), which confirms that changes there are largely carried by the volume transport fluctuations. Several patterns in the Southern Ocean stand out:

(1) A seemingly steady area (over the period 10–15 years back in time, but shown here for only year 15) of positive sensitivities south of the Agulhas current system (between 0 and 45°E, at roughly 50°S). One can speculate that the recirculation in the Agulhas current system would generate disturbances on various timescales. Water masses may be temporarily enclosed within the recirculation, with different instances of "release" leading to different timescales which link this area to 26°N (recirculation regions as "timescale capacitors").
(2) A negative pattern in the South Pacific which an animation reveals to consist of a slowly westward-moving (backward-in-time) dipole of positive and negative sensitivities. Its underlying dynamics are likely the result of a Doppler shift of a westward-propagating Rossby wave by the eastward-flowing ACC (e.g., Hughes, 1995; Fu, 2004; Tulloch et al., 2009). The net dual propagation speed is the wave speed superimposed on the current speed.
(3) Amplitudes are comparable to those in the Atlantic at similar depths, where a dominance of high northern and southern latitudes is discernible. The positive pattern near 50°S around the Prime Meridian is again attributed to the Agulhas current system. A strong positive pattern in the central North Atlantic slowly moves eastward (backward-in-time, not shown).

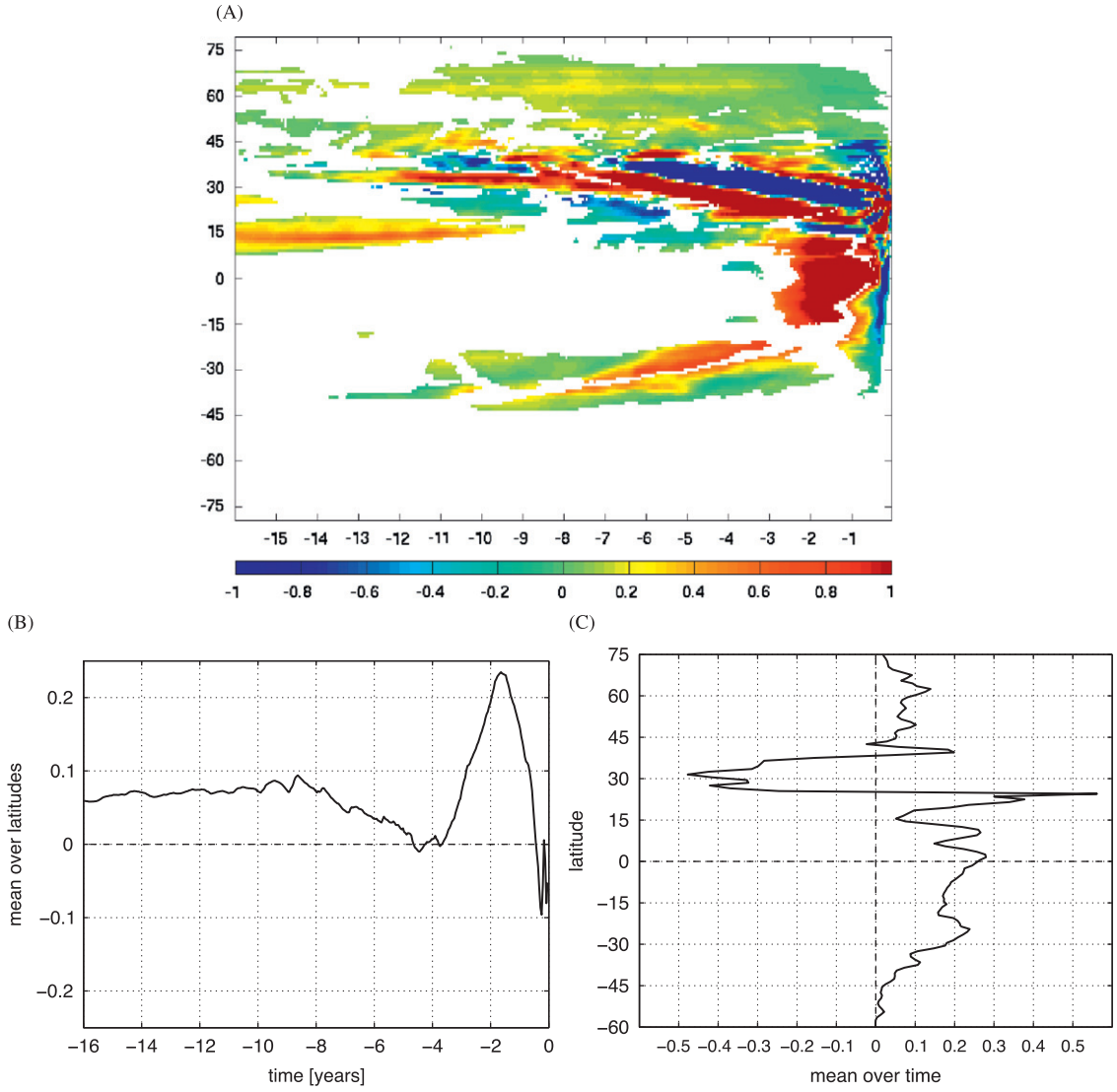

Fig. 11. (A) Latitude vs. time plot at 222 m depth levels of the difference $1/\gamma(\delta J_{MHT}-\delta J_{MVT})$ taken from zonally integrated sensitivities in Fig. 9, and with a range value of $\gamma = 5 \times 10^{-6}$. All signals for which the range of δJ_{MHT} itself is less than 20% of γ are suppressed to focus on sizable signals only. Taking the mean over latitudes or time of panel (A) produces condensed plots (B) and (C), respectively.

The time evolution along specific latitude bands, invoked above, can be summarized via zonal sections as a function of time. Fig. 14 shows such a section through the Antarctic Circumpolar Current (ACC) at 58°S, depicting sensitivities at four different depth levels (the less "noisy" non-optimized solution has been chosen to focus on the broad features). It clearly reveals vertical shear in the ACC (different "tilt" of zonal propagation through time as a function of depth). To the extent that the average ocean depth is 4000 m, and only the top 2000 m is currently subject to frequent in situ measurements (Argo) the sensitivities at depth, both in the Atlantic as well as in the Southern Ocean, appear to point to the importance of obtaining abyssal measurements, if one is interested in capturing relevant contributions to MHT variability on timescales beyond a decade.

3.8. Atmospheric impacts

As mentioned in the introduction, the main purpose of this study is on the ocean's dual space for the purpose of identifying main oceanic pathways and timescales in the context of observing system design. Given the un-coupled nature of our model (ocean-only) we are not able to assess atmospheric pathways and teleconnections. Thus, tightly coupled phenomena, such as the El Nino Southern Oscillation (ENSO) (e.g., Cane, 2010) would only partly be represented by the sensitivity pathways as computed here. Nevertheless, our system does allow for propagation in the ocean interior of sensitivities to surface forcing perturbations. This aspect has recently been studied by Czeschel et al. (2010) who computed multi-decadal sensitivities of the MVT to surface buoyancy forcing in the sub-polar gyre, and identified a pronounced oscillatory sensitivity with a roughly 15–20-year period.

In keeping with our focus on the comparison between MVT and MHC sensitivities for our 16-year state estimate we show, by way of example, zonally integrated sensitivities of MVT and MHT to zonal wind stress perturbations as a function of latitude and time (Fig. 15). The basic structure is very similar to the one in Fig. 9 of near-surface sensitivities to temperature. This reinforces the notion of signal propagation of surface forcing perturbations through Kelvin and Rossby waves. Here, as in Section 3.3 we find the strongest differences between MVT and MHT sensitivities in the tropics out to 3 years, and at northern mid-latitudes up to a decade.

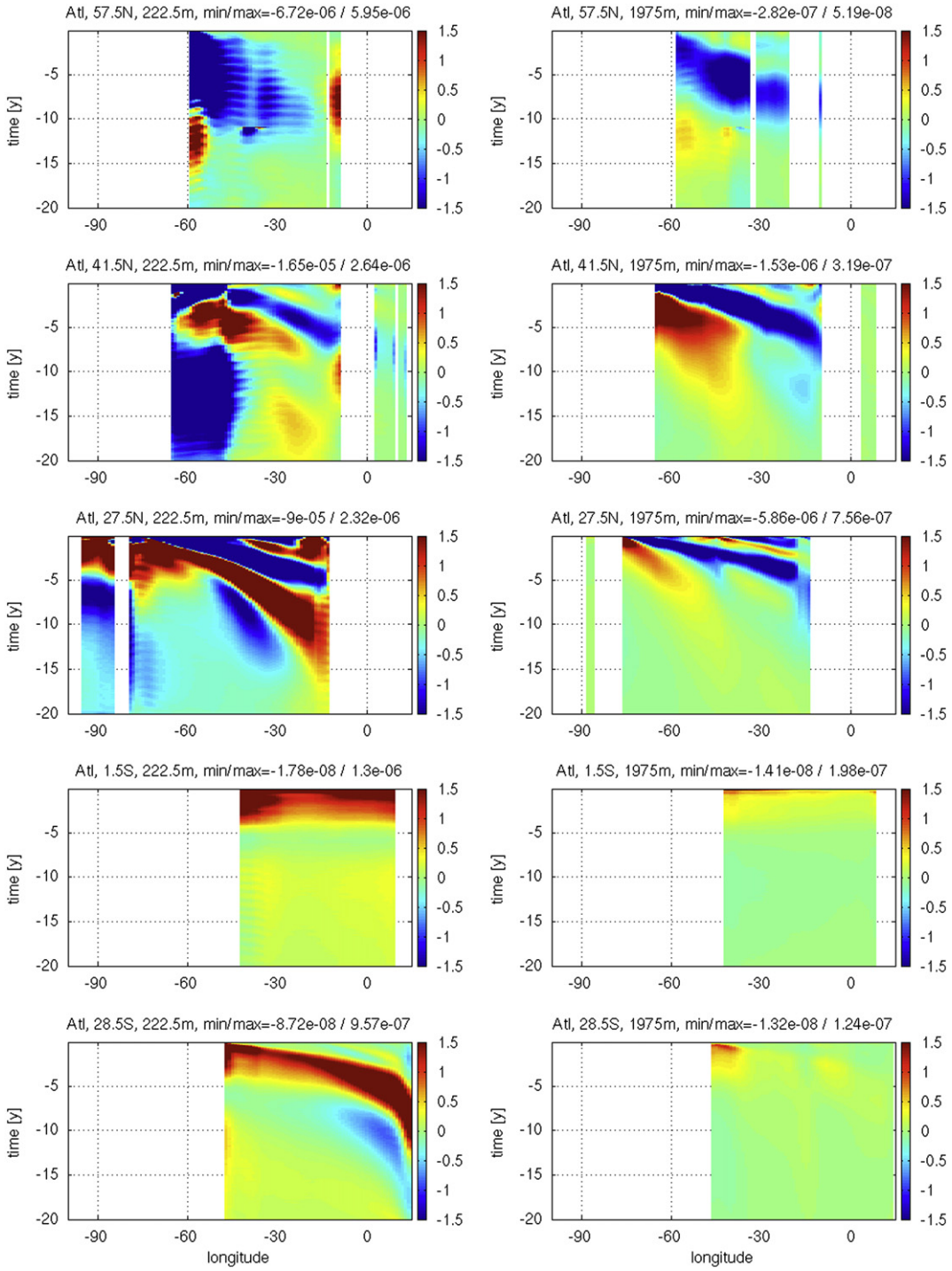

Fig. 12. Same as Fig. 7, but computed from a non-optimized forward model trajectory, and going 20 years back in time.

This is illustrated further by time series taken from Fig. 15 at four latitudes, and shown in Fig. 16. At 26°N, following an initial fast coherent response (less than a year), a strong positive anomaly is visible in MVT but not in MHT sensitivities at 1–4-year timescales. What appears as an oscillation with a negative lobe from 4 to 8 years out in MVT responses (Fig. 15A at 26°N) is not mimicked by MHT responses with a small steady positive sensitivity out to 8 years (Fig. 15B). Strong differences are also apparent at 10°N on short timescales (1–3 years). The pronounced negative–positive lobe apparent in MVT sensitivities is not mirrored by MHT sensitivities. At 60°N, the situation is rather different, with MVT and MHT sensitivities following each other closely. Both exhibit a positive sensitivity anomaly which persists up to a decade. A low frequency behavior is also apparent in the South Atlantic. At 40°S MVT and MHT sensitivities show a coherent 8-year positive anomaly followed by a negative lobe of similar temporal extent. Inspection of Fig. 15 suggests Rossby wave dynamics as a cause.

We emphasize again that no assessment of atmospheric pathways is possible within the given setup, but they are probably significant. The complex spatial sensitivity patterns imply that similarly complex atmospheric forcing patterns may result in rather different responses of the MVT and MHT. In particular, the topic of stochastic optimals in the atmospheric forcing context is

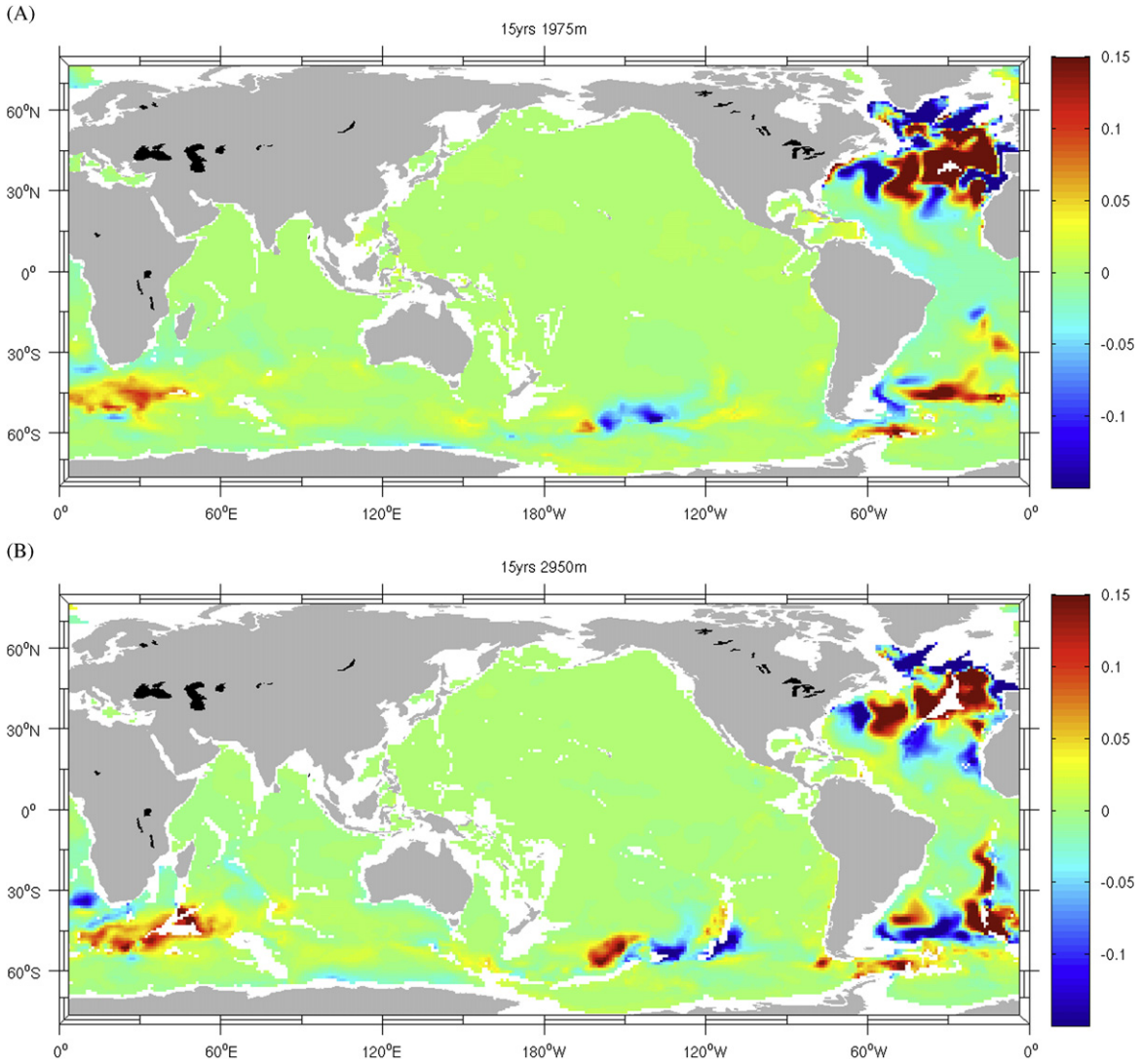

Fig. 13. Normalized MVT response maps similar to those in Fig. 2, but now 15 years backward in time, at depth (A: 1975 m, B: 2950 m), and mostly an order of magnitude smaller. While the overall influence on MVT thus diminishes, the area of influence extend beyond the Atlantic, with significant contributions from various parts of the Southern Ocean.

not touched upon here (but see, e.g., Kleeman and Moore, 1997 for a discussion in the context of ENSO predictability). Detailed knowledge of atmospheric forcing is thus an important ingredient in any ocean observing system which aims at quantifying origins and pathways of ocean circulation changes. However, it can be expected that the oceanographic community can take advantage of the substantial effort already in place for numerical weather prediction, and focus on the oceanographic challenge of filling the vast gaps remaining in ocean observations.

4. Discussion

4.1. Implications for observing system design

No actual observing system has been designed in this study, yet the elements for such a design study have been laid out, and some preliminary conclusions can be drawn.

First, it is evident that a rigorous design study is a complex, yet worthwhile undertaking. Among the most pressing questions are the determination of a set of most relevant, or "most important" (in some form to be agreed upon) metrics which serve as objective functions for sensitivity calculations. An incomplete list among which to choose, are regional (or near-coastal) property transports (zonal or meridional), sea surface temperatures, heat or freshwater content, or sea level. An anticipated outcome, backed up by comparing MVT and MHT, is that sensitivity patterns and timescales will depend on the metric chosen and the region of interest.

A second complicating issue is the choice of regional foci. For example, while the altimetric record suggests a global mean sea-level rise of 3 mm/year from 1993 to present, regional expressions differ greatly, with a 1.5 cm/year rise in the western tropical Pacific accompanied by a 2 mm/year drop in the eastern tropical Pacific, and an ambiguous picture along the US eastern seaboard (Nicholls and Cazenave, 2010).

Third, for a set of given objective functions, sensitivity pathways may be spatially or time-lag correlated, given the basin-mode type structure of many of the patterns. This may provide patterns of redundant information in the sensitivity structure (e.g., significant lag correlations of sensitivity patterns) for different objective functions. In many cases the boundaries serve as an efficient meridional communicator (along with the tropical wave guide as zonal communicator) for dual Kelvin waves. For climate-relevant observations,

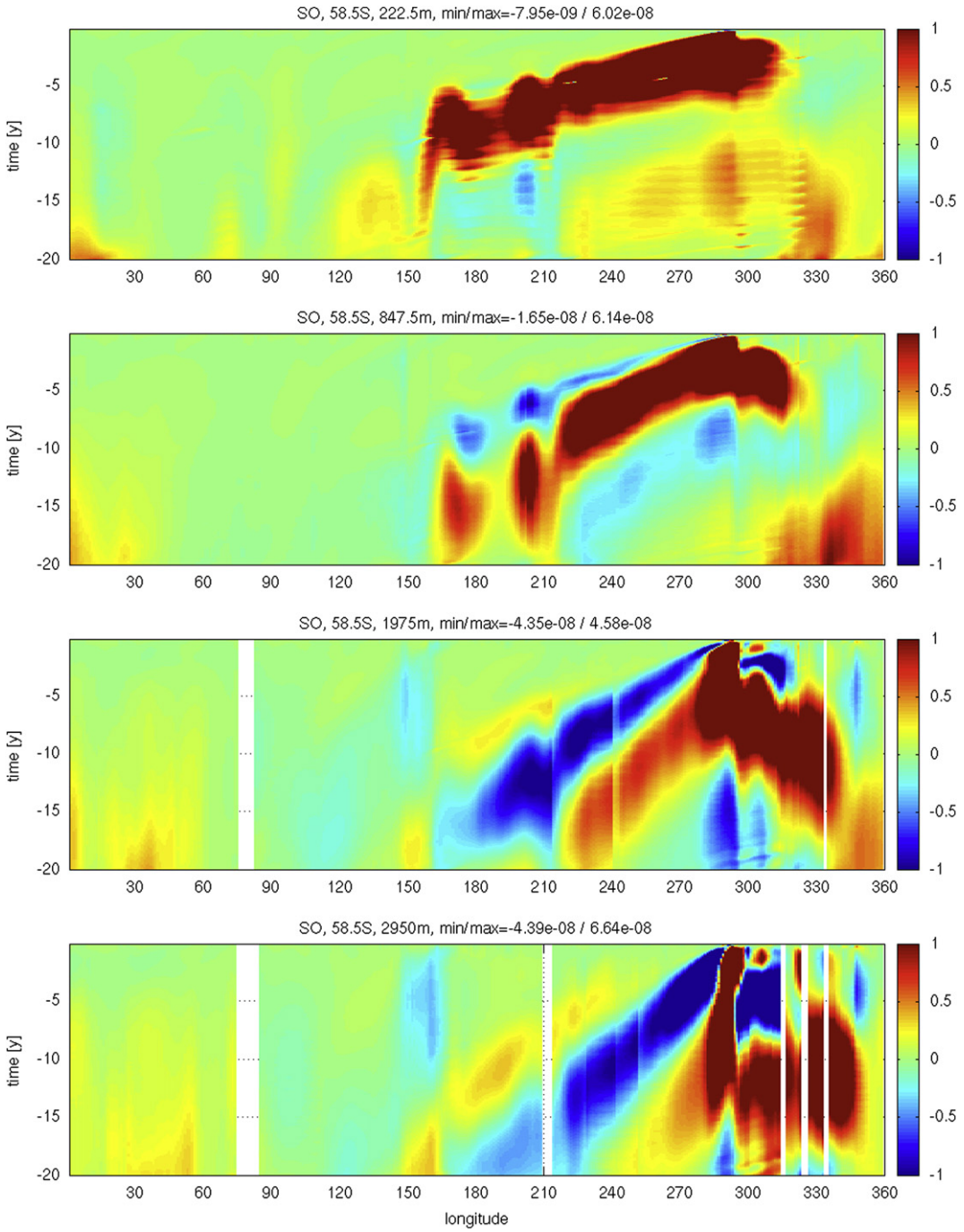

Fig. 14. Meridional lines vs. time, similar to those in Fig. 12, but in the Southern Ocean at 58°S and extended throughout the global latitude circle. Depth levels are, from top-to-bottom, 222, 847, 1975, and 2950 m. A clear westward propagation (backward-in-time) is visible from the Atlantic to the Pacific basin (the connection occurring through the Drake Passage around 70W), whose speed is a function of depth (the increasing "tilt" in the panels from top-to-bottom corresponds to slower propagation).

an important consideration will have to be weigh response amplitudes against expected eddy variability in order to maximize signal-to-noise ratios.

Fourth, the role of the forward state around which the linearized sensitivities were calculated needs to be carefully assessed.

Fifth, the results will have to be considered in the light of technological capabilities and costs. A particularly troubling element in this regard is the deep sensitivities in the South Atlantic and their spreading into the Southern Ocean at long lead times (here considered 15 years, see Fig. 13). Apart from difficulties stemming from the remoteness of the region (the Southern Ocean remains sparsely sampled even today), obtaining the relevant deep observations would be technologically difficult and programmatically challenging because of the long-term commitment required for their maintenance.

In the context of past observations, another consequence is that reconstructing heat and volume transport variability on decadal timescales and beyond from past observations may be limited by the sparse sampling of the Southern Ocean. Similarly troubling are the complementarity of salinity vs. temperature sensitivities (their tendency to compensate for density) in view of the much more limited number of salinity observations available in the past, compared to those for temperature (XBTs).

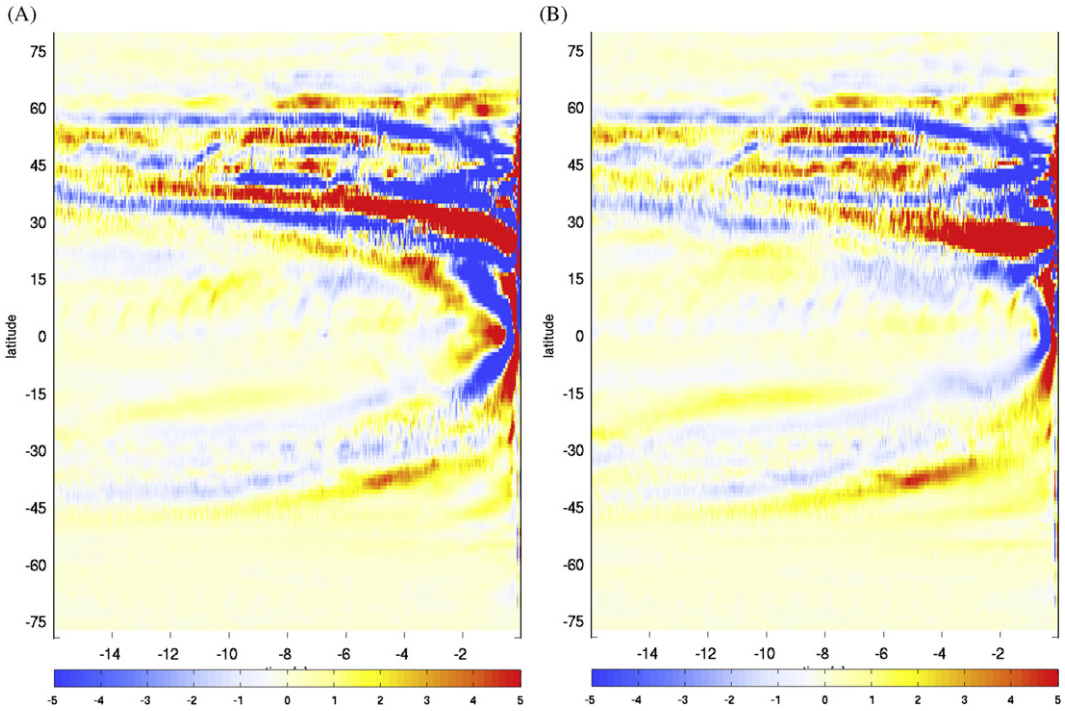

Fig. 15. Zonally integrated normalized responses for MVT (A) and MHT (B) to zonal wind stress perturbations as a function of time and latitude in the Atlantic (comparable to those of 222 m temperature responses, Fig. 9).

The richness of the time-evolving dual state space is evidently comparable to that of the forward state. It implies that extensive analyses are required and care has to be taken in interpreting the patterns inferred. Conclusions drawn depend on various "weights" (implicit or explicit) and require close consultation between the modeling and the observational community. Thus, what emerges may be considered as a long-term program for conducting quantitative observing system design.

4.2. Preliminary conclusions

The major purpose here has been to demonstrate that the sensitivity of major elements of the climate system to temporal and regional disturbances in the ocean state can be readily determined using dual models, that the results are interesting and physically plausible. Although a somewhat arbitrary subset of the enormous number of possibilities for observing climate-related shifts in the ocean has been selected, and no observational system has actually been designed, some useful conclusions are possible:

(1) The dual state provides valuable information, complementary to the forward model state, and whose detailed analysis is both rewarding and as challenging as the analysis of the forward GCM. The complementarity is most visible in the role of Kelvin and Rossby wave propagation in setting barotropic and baroclinic adjustment timescales, as discussed, e.g., by Johnson and Marshall (2002, 2004).

(2) In the context of the observation and the monitoring of key climate indices such as meridional heat or volume transports at specific sections, significant sensitivities of similar magnitude are not purely local, but extend throughout the Atlantic on timescales up to 10 years, with signals emanating from increasingly remote places. For example, Fig. 2 indicates that at 4 years back in time, several remote "centers-of-action" conspire to influence the MVT at 26°N.

(3) Responses in seemingly similar climate indices such as those investigated here (J_{MHT} vs. J_{MVT}, 26 vs. 48°N) may differ substantially in (scaled) amplitude and sign and as a function of time, making it difficult to infer responses of one quantity from those of the other. One must carefully consider which indices are the most relevant in the context of climate monitoring (or prediction). In particular, interchangeable use of MVT and MHT variability obscures the underlying causal processes.

(4) Transient sensitivities are dual manifestations of dynamical processes underlying the global oceanic teleconnections discussed in the context of climate variability (e.g., Liu and Alexander, 2007). The schematic presented in Fig. 5 shows some timescales of what could be termed dual teleconnections. Among the striking features are fast timescales connecting 26°N in the Atlantic (a) to the near-surface Southern Ocean west of Cape Horn and the western tropical Pacific (O(4) and O(6) years, respectively), and (b) to the (tropical) Indian Ocean (O(7)) years. The latter has to come through the link of dual Kelvin waves along the east and west coast of South America, the tropical Pacific, and leaking through the Indonesian passages.

(5) Also noteworthy is that in none of the results presented, did the high northern latitudes of the North Atlantic stand out as dominating regions of sensitivities (but notice the lack of an Arctic ocean in the model). This result may appear surprising, given the prominent role ascribed to these regions in the literature as apparent key regions influencing MVT and MOC variability.

(6) A contribution to MVT variability discussed recently by Biastoch et al. (2008) on timescales of half a decade involves eddy shedding in the Agulhas retroflection region, propagating westward in the South Atlantic toward the coast of Brazil, advecting northward with the Brazil current and connecting with the Gulf Stream. Although our model does not resolve such eddies, there is clear evidence for such a South Atlantic link (but here represented by Rossby and Kelvin waves) within the thermocline in the results.

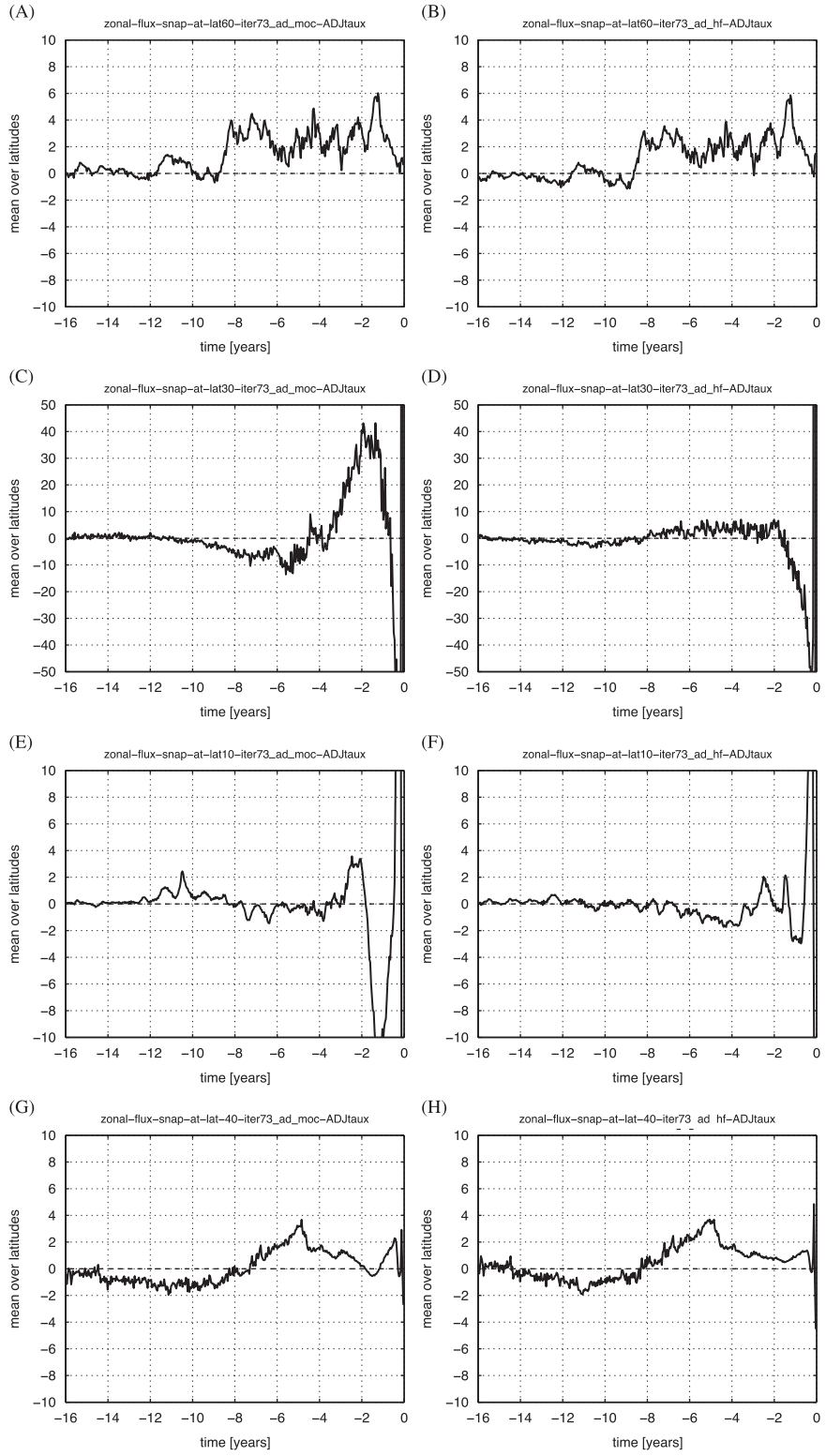

Fig. 16. Time series of MVT (left) and MHT (right) responses to zonal wind stress perturbations at various latitude sections, extracted from fields depicted in Fig. 15: (A) MVT 60°N, (B) MHT 60°N, (C) MVT 30°N, (D) MHT 30°N, (E) MVT 10°N, (F) MHT 10°N, (G) MVT 40°S and (H) MHT 40°S.

(7) A clear exposure of the Doppler effect in the Southern Ocean which the fast eastward-flowing ACC exerts on westward-propagating Rossby waves (for zero mean flow) and which leads to Doppler-shifted eastward Rossby wave propagation (e.g., Hughes, 1995; Fu, 2004; Tulloch et al., 2009, but see also Chelton et al., 2007 for caveats in the presence of eddies and their eastward advection by the ACC).

Table 1 provides some numbers for hypothetical perturbations in various regions and at different instances in time. The next-to-last column shows changes in MHT (in PW) for perturbations applied near-surface (around 222 m depth) over various geographical regions (columns 1–3). The fourth column lists the prior uncertainty, σ, that sets the perturbation amplitude chosen. Values of $\delta J = 0.04$ PW indicate a roughly 4% change in MHT

Table 1
A list of anticipated changes in MHT inferred from adjoint sensitivities to temperature for several instances back in time (fourth column) and perturbation regions. Perturbed MHT was calculated applying near-surface (222 m, next-to-last column) and deep (1975 m, last column) temperature perturbations, integrating sensitivity fields over an area given by LAT (second column) and LON (third column), and applying a common thickness of dz=500 m. Reference MHT is $\bar{J}_{MHT} = 1.1$ PW.

Region	LAT	LON	Time (yr)	δJ at 222 m (PW)	δJ at 1975 m (PW)
NW sub-polar	45–60°N	75–15°W	1	−0.048	−0.022
			4	−0.032	−0.029
			7	−0.041	−0.009
NE sub-tropics	15–30°N	30–0°W	1	0.010	-4.3×10^{-4}
			4	−0.028	−0.006
			7	0.025	−0.0015
Equator	5°S–5°N	45–0°W	1	0.030	0.007
			4	0.009	0.002
			7	9.2×10^{-4}	−0.001
SE sub-tropics	40–25°S	0–15°E	1	-9.6×10^{-4}	-1.9×10^{-4}
			4	0.020	0.002
			7	0.024	0.001

compared to the reference value of $\bar{J}_{MHT} = 1.1$ PW. Local and remote regions contribute similar amounts to MHT variations. For example, changes in MHT due to temperature perturbations in the northwest sub-polar Atlantic 7 years backward-in-time exceed those due to temperature changes in the northeast sub-tropics 1–4 years earlier in time. Furthermore, the latter are comparable to MHT changes arising from perturbations in the southeast sub-tropical Atlantic 4–7 years back in time. Temperatures at depth (chosen here as 1975 m) lead, overall, to smaller MHT changes, but are of increasingly remote origin.

The sensitivity analyses presented here delineate a method to describe and quantify causal connections (pathways, timescales, and response amplitudes) between climate diagnostics (here Atlantic MVT and MHT), the large-scale circulation and the forcings. On timescales of years to decades, a spatial pattern emerges which identifies various potential centers-of-action that conspire in influencing variations in those climate diagnostics. Up to roughly a decade wave-like adjustment processes dominate in amplitude. Beyond a decade, effects of advection may become important. On shorter timescales advection may be relevant in modulating wave propagation. The cautionary note by, e.g., Bingham et al. (2007) of limited information content in MOC recordings at any one latitude for determining the overall North Atlantic circulation is supported by our transient sensitivity results.

A general limitation of this study is that the model resolution does not admit or resolve mesoscale eddies. Whereas many of the identified signals are here interpreted in terms of wave dynamics, high-resolution simulations suggest a significant role for eddies, e.g., in exchange processes between the sub-polar and sub-tropical North Atlantic, the link between the Indian Ocean and the North Atlantic via the Agulhas retroflection, variability in the Brazil current, or the dynamics of the ACC. Future work should assess to which extent inferred sensitivities carry over to eddy-admitting or fully resolving resolutions. Such work will have to address the difficult question of distinguishing between (non-linear) eddy-induced effects, and those carried by (linear) Rossby wave propagation, both of which travel at roughly the same speed (Chelton et al., 2007; Tulloch et al., 2009). Similarly, the role of sharply defined continental boundary regions in supporting boundary wave propagation may be underestimated in coarse-resolution models, as pointed out by Greatbatch and Peterson (1996). While our study shows the crucial link that these regions provide in terms of "dynamic" teleconnections, an improved representation of the coastal and shelf-wave guide is clearly warranted.

To the extent that pathways are robust, and sensitivity (or response) amplitudes broadly reasonable, the sensitivity maps may provide clues as to which regions are of heightened importance for taking relevant observations. No model is completely realistic and the present one is no exception. Nonetheless, many of the dominant sensitivities are robust because they are dependent upon physically plausible ocean dynamics.

This analysis can be extended in numerous ways: to longer times; with the use of higher resolution models; to explore sensitivities to meteorological forcing of the present and past; to the use of different target functions; to model elements themselves (mixing coefficients, water depths, etc.), and in particular to fuller exploration of the dynamics of the dual system. On very long timescales, such work has already been performed with the analysis of "equilibrium sensitivities" (Bugnion et al., 2006a,b).

Very recently, Czeschel et al. (2010) have investigated multi-decadal sensitivities to surface forcing in a regional Atlantic configuration of the MITgcm at comparable resolution. Because meteorological observations are already near-global in scope, and likely to continue to be so, sensitivity to atmospheric forcing is somewhat less urgent in the experimental design context than are the more regional oceanographic observing systems. In a similar spirit, Heimbach et al. (2010) have also demonstrated the power of the dual space approach to infer sensitivities of sea ice export through the Canadian Arctic Archipelago on interannual timescales using a coupled ocean/sea ice adjoint model.

As for the dual system, singular vectors which shed light on regions and mechanisms of non-normal transient amplification of the chosen diagnostic (formulated as a norm kernel) hold the prospect of sharpening some of the analyses presented here (Farrell, 1988; Trefethen et al., 1993). While patterns are likely similar to adjoint sensitivities, perturbation patterns that are projected onto the adjoint fields are those which optimize the norm kernel over a certain time, rather than those of estimated variability as chosen here. Perhaps a clearer decomposition is obtained in terms of such optimal perturbation patterns, and work in this regard has been undertaken in the context of the MITgcm by Zanna et al. (2010, 2011, submitted for publication). These point to regions of the highest uncertainties with regard to observations of the target diagnostic. An important direction of research will be the extension of this work to realistic configurations. Similar methods have been successfully applied to targeted observations in numerical weather prediction (Buizza and Palmer, 1995; Gelaro et al., 1999) and in the context of ENSO dynamics and predictability (Penland and Sardeshmukh, 1995;

Moore and Kleeman, 1997). Approaches to approximate full singular vector calculations through the use of eigenmodes of the linearized model operator have also been pursued in the context of realistic GCM configurations (Sevellec et al., 2008).

The issue of the climate diagnostic elements is perhaps the most difficult one. Here two indices (MHT, MVT) were adopted, and, as expected, are closely related. Nonetheless they exhibit markedly different response patterns, especially in the vicinity of the correspondingly arbitrary latitude used (26°N). Other diagnostics, such as upper ocean heat content, Drake Passage transport, regional sea level, etc., need to be explored in similar fashion if they are regarded as candidates for dominant elements of climate change.

Acknowledgments

We are grateful for useful comments from Martin Losch, and from two anonymous reviewers. Supported in part through the "Estimating the Circulation and Climate of the Ocean" (ECCO) and the "Atlantic MOC Observing System Studies Using Adjoint Models" projects of National Oceanographic Partnership Program (NOPP) with funding from NASA, and the NSF Collaboration in Mathematics and Geoscience (CMG) project "Uncertainty Quantification in Geophysical State Estimation". Computing support came through facilities at the NASA Advanced Supercomputing (NAS) division and the NCAR Scientific Computing Division (SCD).

Appendix. Model configuration

The calculations were performed with the MIT general circulation model (MITgcm) (Marshall et al., 1997a,b; Adcroft et al., 2002) in the ECCO-GODAE version 3 configuration (Wunsch et al., 2007; Wunsch and Heimbach, 2009). It is characterized by a quasi-global domain covering 80°N–80°S at a $1^\circ \times 1^\circ$ horizontal resolution with 23 unevenly spaced height levels. Vertical mixing is parameterized using the KPP scheme of Large et al. (1994), isopycnal diffusion and eddy transport are parameterized using the Gent–McWilliams/Redi schemes (Gent and McWilliams, 1990; Redi, 1982). The surface forcing is achieved with the Large and Yeager (2004) bulk formulae which convert surface atmospheric state variables into air–sea fluxes. A dynamic/thermodynamic sea ice model computes sea ice concentration, snow and ice thickness, ice velocities, and modifies air–sea fluxes over ice-covered regions (Losch et al., 2010). The model is integrated from January 1992 to December 2007 using adjusted initial conditions and surface atmospheric state variables. These adjustments are the result of a least-squares fit of the model to a variety of observations using the adjoint or Lagrange multiplier method (for a list of observations used, see Wunsch et al., 2009). The surface boundary conditions consist of 6-hourly atmospheric state variables from the NCEP/NCAR reanalysis (Kalnay et al., 1996) with superimposed daily adjustments of surface air temperature, specific humidity, precipitation, downwelling shortwave radiation, and wind speed vector.

The adjoint model required both for the gradient-based optimization as well as for the sensitivity calculations was generated via automatic differentiation (AD, see, e.g., Marotzke et al., 1999; Heimbach et al., 2005; Griewank and Walther, 2008). Sensitivity calculations using the optimized solution are based on the adjoint model generated with the commercial AD tool TAF (Giering et al., 2005). For the non-optimized solution we generated the adjoint both via TAF as well as the open-source tool OpenAD (Utke et al., 2008). Both AD-generated models show essentially the same results (as part of the routine test suite of the MITgcm, adjoint models are now being generated on a nightly basis both with TAF and OpenAD to ascertain that their results agree).

In addition to assessing the impact of the reference trajectory itself (optimized vs. non-optimized) we also assessed the omission of some of the physics in the adjoint model. The adjoint of the optimized solution is approximate in the sense that sensitivities related to the parameterization schemes are omitted. For the non-optimized sensitivity calculation we omitted the KPP scheme in both the forward and adjoint calculation, but kept the GM/Redi scheme active both in the forward as well as the adjoint simulation, i.e., we ran an exact adjoint model.

References

Adcroft, A., Campin, J.-M., Heimbach, P., Hill, C., Marshall, J., 2002. MITgcm Release1 Manual (Online Documentation). MIT/EAPS, Cambridge, MA 02139, USA.

Biastoch, A., Böning, C.W., Lutjeharms, J.R.E., 2008. Agulhas leakage dynamics affects decadal variability in Atlantic overturning circulation. Nature 456, 489–492. doi:10.1038/nature07426.

Bingham, R.J., Hughes, C.W., Roussenov, V., Williams, R.G., 2007. Meridional coherence of the North Atlantic meridional overturning circulation. Geophys. Res. Lett. 34, L23606.

Bugnion, V., Hill, C., Stone, P., 2006a. An adjoint analysis of the meridional overturning circulation in an ocean model. J. Clim. 19 (15), 3732–3750.

Bugnion, V., Hill, C., Stone, P., 2006b. An adjoint analysis of the meridional overturning circulation in a hybrid coupled model. J. Clim. 19 (15), 3751–3767.

Buizza, R., Palmer, T.N., 1995. The singular-vector structure of the atmospheric global circulation. J. Atmos. Sci. 52, 1434–1456.

Cane, M.A., 2010. The El Niño-Southern Oscillation Phenomenon. Cambridge University Press, London.

Cessi, P., Bryan, K., Zhang, R., 2004. Global seiching of thermocline waters between the Atlantic and the Indian–Pacific ocean basins. Geophys. Res. Lett. 31, L04302.

Cessi, P., Otheguy, P., 2003. Oceanic teleconnections: remote response to decadal wind forcing. J. Phys. Oceanogr. 33, 1604–1617.

Chelton, D., Schlax, M.G., Samelson, R.M., De Szoeke, R.A., 2007. Global observations of large oceanic eddies. Geophys. Res. Lett. 34, L15606. doi:10.1029/2007GL030812.

Chelton, D.B., Schlax, M.G., 1996. Global observations of oceanic Rossby waves. Science 272, 234–238.

Cunningham, S.A., Kanzow, T., Rayner, D., Baringer, M.O., Johns, W.E., Marotzke, J., Longworth, H.R., Grant, E.M., Hirschi, J.J.-M., Beal, L.M., Meinen, C.S., Bryden, H.L., 2007. Temporal variability of the Atlantic meridional overturning circulation at 26.5°N. Science 317, 935–938. doi:10.1126/science.1141304.

Czeschel, L., Marshall, D.P., Johnson, H.L., 2010. Oscillatory sensitivity of Atlantic overturning to high-latitude forcing. Geophys. Res. Lett. 37, L10601. doi:10.1029/2010GL043177.

Farrell, B.F., 1988. Optimal excitation of neutral Rossby waves. J. Atmos. Sci. 45, 163–172.

Forget, G., Wunsch, C., 2007. Global hydrographic variability and the data weights in oceanic state estimates. J. Phys. Oceanogr. 37 (8), 1997–2008. doi:10.1175/JPO3072.1.

Fu, L.-L., 2004. Latitudinal and frequency characteristics of the westward propagation of large-scale oceanic variability. J. Phys. Oceanogr. 34, 1907–1921.

Fukumori, I., Menemenlis, D., Lee, T., 2006. A near-uniform basin-wide sea level fluctuation of the Mediterranean Sea. J. Phys. Oceanogr. 37, 338–358.

Galanti, E., Tziperman, E., 2003. A midlatitude-ENSO teleconnection mechanism via baroclinically unstable long Rossby waves. J. Phys. Oceanogr. 33, 1877–1887.

Gelaro, R., Langland, R.H., Rohali, G.D., Rosmond, T.E., 1999. An assessment of the singular-vector approach to targeted observations using the FASTEX dataset. Q. J. R. Meteorol. Soc. 125, 3299–3327.

Gent, P.R., McWilliams, J.C., 1990. Isopycnal mixing in ocean circulation models. J. Phys. Oceanogr. 20, 150–155.

Giering, R., Kaminski, T., 1998. Recipes for adjoint code construction. ACM Trans. Math. Software 24, 437–474.

Giering, R., Kaminski, T., Slawig, T., 2005. Generating efficient derivative code with TAF: adjoint and tangent linear Euler flow around an airfoil. Future Gener. Comput. Syst. 21 (8), 1345–1355.

Greatbatch, R.J., Peterson, K.A., 1996. Interdecadal variability and oceanic thermohaline adjustment. J. Geophys. Res. 101 (C9), 20467–20482.

Griewank, A., Walther, A., 2008. Evaluating derivatives principles and techniques of algorithmic differentiation. In: Frontiers in Applied Mathematics, second ed., vol. 19. SIAM, Philadelphia, 442 pp.

Haine, T.W.N., Zhang, H., Waugh, D.W., Holzer, M., 2008. On transit-time distributions in unsteady circulation models. Ocean Modelling 21, 35–45. doi:10.1016/j.ocemod.2007.11.004.

Haine, T.W.N., Hall, T.M., 2002. A generalized transport theory: water-mass composition and age. J. Phys. Oceanogr. 32, 1932–1946.

Heimbach, P., 2008. The MITgcm/ECCO adjoint modelling infrastructure. CLIVAR Exchanges 44 13 (1), 13–17.

Heimbach, P., Hill, C., Giering, R., 2005. An efficient exact adjoint of the parallel MIT general circulation model, generated via automatic differentiation. Future Gener. Comput. Syst. 21 (8), 1356–1371. doi:10.1016/j.future.2004.11.010.

Heimbach, P., Menemenlis, D., Losch, M., Campin, J.M., Hill, C., 2010. On the formulation of sea-ice models. Part 2: lessons from multi-year adjoint sea-ice export sensitivities through the Canadian Arctic Archipelago. Ocean Modelling 33 (1–2), 145–158. doi:10.1016/j.ocemod.2010.02.002.

Holzer, M., Hall, T.M., 2000. Transit-time and tracer-age distributions in geophysical flows. J. Atmos. Sci. 57, 3539–3558.

Hughes, C.W., 1995. Rossby waves in the Southern Ocean: a comparison of TOPEX/Poseidon altimetry with model predictions. J. Geophys. Res. 100, 15933–15950.

Johnson, H.L., Marshall, D.P., 2002. A theory for the surface Atlantic response to thermohaline variability. J. Phys. Oceanogr. 32, 1121–1132.

Johnson, H.L., Marshall, D.P., 2004. Global teleconnections of meridional overturning circulation anomalies. J. Phys. Oceanogr. 34, 1702–1722.

Kalnay, E., et al., 1996. The NCEP/NCAR 40-year reanalysis project. Bull. Am. Meteorol. Soc. 77 (3), 437–471.

Kanzow, T., Cunningham, S.A., Rayner, D., Hirschi, J.J.-M., Johns, W.E., Baringer, M.O., Bryden, H.L., Beal, L.M., Meinen, C.S., Marotzke, J., 2007. Observed flow compensation associated with the MOC at 26.5°N in the Atlantic. Science 317, 938–941. doi:10.1126/science.1141304.

Khatiwala, S., 2007. Computational framework for simulation of biogeochemical tracers in the ocean. Glob. Biogeochem. Cycles 21, GB3001. doi:10.1029/2007GB002923.

Killworth, P.D., Chelton, D.B., De Szoeke, R.A., 1997. The speed of observed and theoretical long extratropical planetary waves. J. Phys. Oceanogr. 27, 1946–1966.

Kleeman, R., Moore, A.M., 1997. A theory for the limitation of ENSO predictability due to stochastic atmospheric transients. J. Atmos. Sci. 54, 753–767.

Köhl, A., 2005. Anomalies of meridional overturning: mechanisms in the North Atlantic. J. Phys. Oceanogr. 35 (8), 1455–1472. doi:10.1175/JPO2767.1.

Lanczos, C., 1961. Linear Differential Operators. Van Nostand, New York.

Large, W.G., McWilliams, J.C., Doney, S.C., 1994. Oceanic vertical mixing: a review and a model with nonlocal boundary layer parameterization. Rev. Geophys. 32, 363–403.

Large, W.G., Yeager, S.G., 2004. Diurnal to decadal global forcing for ocean and sea-ice models: the data sets and flux climatologies. Technical Note NCAR/TN-460+STR, NCAR, Boulder, CO.

Liu, Z., Alexander, M., 2007. Atmospheric bridge, oceanic tunnel, and global climatic teleconnections. Rev. Geophys. 45, RG2005.

Losch, M., Menemenlis, D., Campin, J.M., Heimbach, P., Hill, C., 2010. A dynamic–thermodynamic sea ice model for ocean climate modeling on an Arakawa C-grid: part 1: forward model sensitivities. Ocean Modelling 33 (1–2), 129–144. doi:10.1016/j.ocemod.2009.12.008.

Marotzke, J., Giering, R., Zhang, K.Q., Stammer, D., Hill, C., Lee, T., 1999. Construction of the adjoint MIT ocean general circulation model and application to Atlantic heat transport variability. J. Geophys. Res. 104 (C12), 29529–29547.

Marshall, J., Adcroft, A., Hill, C., Perelman, L., Heisey, C., 1997b. A finite-volume, incompressible Navier Stokes model for studies of the ocean on parallel computers. J. Geophys. Res. 102 (C3), 5753–5766.

Marshall, J., Hill, C., Perelman, L., Adcroft, A., 1997a. Hydrostatic quasi-hydrostatic and nonhydrostatic ocean modeling. J. Geophys. Res. 102 (C3), 5733–5752.

Moore, A.M., Kleeman, R., 1997. The singular vectors of a coupled ocean–atmosphere model of ENSO. I: thermodynamics, energetics and error growth. Q. J. R. Meteorol. Soc. 123, 953–981.

Morse, P.M., Feshbach, H., 1953. Methods of Theoretical Physics. McGraw-Hill, New York.

Nicholls, R.J., Cazenave, A., 2010. Sea-level rise and its impact on coastal zones. Science 328, 1517–1520. doi:10.1126/science.1185782.

Penland, C., Sardeshmukh, P.D., 1995. The optimal growth of tropical sea surface temperature anomalies. J. Clim. 8 (8), 1999–2024.

Primeau, F., Deleersnijder, E., 2009. On the time to tracer equilibrium in the global ocean. Ocean Sci. 5, 13–28.

Redi, M.H., 1982. Oceanic isopycnal mixing by coordinate rotation. J. Phys. Oceanogr. 12, 1154–1158.

Schröter, J., Wunsch, C., 1986. Solution of nonlinear finite difference ocean models by optimization methods with sensitivity and observational strategy analysis. J. Phys. Oceanogr. 16, 1855–1874.

Sevellec, F., Huck, T., Jelloul, M.B., Grima, N., Viadard, J., Weaver, A., 2008. Optimal surface salinity perturbations of the meridional overturning and heat transport in a global ocean general circulation model. J. Phys. Oceanogr. 38, 2739–2754.

Stammer, D., 2008. Response of the global ocean to Greenland and Antarctic ice melting. J. Geophys. Res. 113, C06022.

Trefethen, L.N., Trefethen, A.E., Reddy, S.C., Driscoll, T.A., 1993. Hydrodynamic stability without eigenvalues. Science 261, 578–584. doi:10.1126/science.261.5121.578.

Tulloch, R., Marshall, J., Smith, K.S., 2009. Interpretation of the propagation of surface altimetric observations in terms of planetary waves and geostrophic turbulence. J. Geophys. Res. 114, C02005. doi:10.1029/2008JC005055.

Utke, J., Naumann, U., Fagan, M., Tallent, N., Strout, M., Heimbach, P., Hill, C., Ozyurt, D., Wunsch, C., 2008. OpenAD/F: a modular open source tool for automatic differentiation of Fortran codes. ACM Trans. Math. Software 34 (4).

Veronis, G., Stommel, H., 1956. The action of variable wind stresses on a stratified ocean. J. Mar. Res. 15, 43–75.

Wunsch, C., 2006. Discrete Inverse and State Estimation Problems: with Geophysical Fluid Applications. Cambridge University Press, Cambridge, UK, 400 pp.

Wunsch, C., Heimbach, P., 2007. Practical global oceanic state estimation. Physica D 230 (1–2), 197–208.

Wunsch, C., Heimbach, P., 2008. How long to oceanic tracer and proxy equilibrium? Q. Sci. Rev. 28, 637–651.

Wunsch, C., Heimbach, P., 2009. The globally integrated ocean circulation (MOC), 1992–2006: seasonal and decadal variability. J. Phys. Oceanogr. 39 (2), 351–368.

Wunsch, C., Heimbach, P., Ponte, R.M., Fukumori, I., 2009. The global general circulation of the oceans estimated by the ECCO-Consortium. Oceanography 22 (2), 88–103.

Wunsch, C., Ponte, R.M., Heimbach, P., 2007. Decadal trends in sea level patterns: 1993–2004. J. Clim. 20 (24), 5889–5911.

Zanna, L., Heimbach, P., Moore, A.M., Tziperman, E., 2010. Optimal growth of tropical Atlantic SST anomalies. J. Phys. Oceanogr. 40 (5), 983–1003. doi:10.1175/2009JPO4196.1.

Zanna, L., Heimbach, P., Moore, A.M., Tziperman, E., 2011. Optimal excitation of interannual Atlantic meridional overturning circulation variability. J. Clim. 24 (2), 413–423. doi:10.1175/2010JCLI3610.1.

Zanna, L., Heimbach, P., Moore, A.M., Tziperman, E. Analysis of the predictability and variability of the Atlantic ocean in response to optimal surface excitation. Q. J. R. Meteorol. Soc., submitted for publication.